









Investigation of the ameliorative effects of amygdalin against arsenic trioxide-induced cardiac toxicity in rat

Haochuan Guo ^{a,1}, Yanfei Ouyang ^{b,1}, Yuxia Wang ^a, Keqian He ^a, Mengwei Zhao ^a, Zhihong Ma ^a,
Yongxing Song ^{a,c}  , Hongfang Wang ^{a,c}  , Donglai Ma ^{a,c,d}  

Show more 

 Outline |  Share  Cite

<https://doi.org/10.1016/j.jff.2025.106795> 

[Get rights and content](#) 

Under a Creative Commons [license](#) 

[Open access](#)

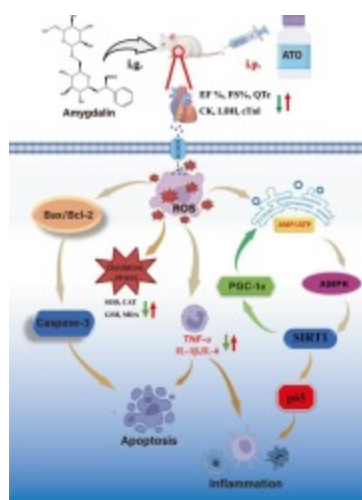
Highlights

- Amygdalin's Antioxidant and Anti-Inflammatory Effects.
- Cardioprotective Mechanisms Against Arsenic Trioxide (ATO).
- Histopathological and Biomarker Improvements.
- Modulation of AMPK/SIRT1 Pathway and Inflammation Reduction.

Abstract

AMG, recognized as vitamin B17, is celebrated for its antioxidant and anti-inflammatory prowess, which underpins its utility in averting disease and decelerating the aging process. This study ventures to elucidate the cardioprotective mechanisms of amygdalin against ATO-induced cardiac injury, with a spotlight on the AMPK and SIRT1 signaling cascade. Employing a Sprague-Dawley rat model, we administered amygdalin followed by ATO and conducted a 15-day longitudinal study. Our findings underscore the ameliorative impact of amygdalin on histopathological cardiac anomalies, a reduction in cardiac biomarkers, and an invigoration of antioxidant defenses, thereby attenuating oxidative stress and inflammation. Notably, amygdalin's intervention abrogated ATO-induced apoptosis and inflammatory cascades, modulating key proteins along the AMPK/SIRT1 pathway and significantly dampening inflammation. Collectively, these insights advocate for amygdalin's role as a guardian against ATO-induced cardiotoxicity, potentially through the activation of the AMPK/SIRT1 axis, offering a novel therapeutic vista in mitigating oxidative stress, apoptosis, and inflammation.

Graphical abstract



[Download: Download high-res image \(98KB\)](#)

[Download: Download full-size image](#)

[<](#) Previous

Next [>](#)

Keywords

Amygdalin; Arsenic trioxide; Cardiac toxicity; Inflammation; Apoptosis; AMPK/SIRT1/ PGC-1 α

Abbreviations

APL, Acute promyelocytic leukemia; ATO, Arsenic trioxide; AMG, Amygdalin; AMPK, Adenosine 5'-monophosphate -activated protein kinase; SIRT1, Sirtuin-1; PGC-1 α , Peroxisome proliferators-activated receptor γ coactivator lalpha; NF- κ B, Nuclear factor kappa-B; ROS, Reactive oxygen species; TNF- α , Tumor necrosis factor- α ; IL-1 β , Interleukin-1beta; IL-6, Interleukin-6; ECG, Electrocardiogram; EF, Ejection fraction; FS, Fractional shortening; LVESV, Left ventricular end-systolic volume; LVEDV, Left ventricular end-diastolic volume; CK, Creatine kinase; LDH, Lactate dehydrogenase; cTnI, Cardiac troponin I; MDA, Malondialdehyde; SOD, Superoxide dismutase; GSH, Glutathione; CAT, Catalase; NS, Normal saline

1. Introduction

Arsenic trioxide (ATO), with its deep roots in traditional Chinese medicine, has ascended to prominence as a preeminent therapeutic agent in the targeted treatment of acute promyelocytic leukemia (APL) (Fox et al., 2008; Hofmann et al., 2020). The efficacy of ATO extends to the oncological domain, where it has been lauded for its potency against hepatic malignancies and a spectrum of neoplastic growths (Yang, Wang, Shi, Zhao, & Li, 2022; Zhang et al., 2021). Despite its clinical successes, the protracted exposure to even therapeutic concentrations of ATO poses a significant risk of cardiotoxicity, manifesting as QT interval prolongation and the potential for sudden cardiac demise (Vineetha & Raghu, 2019; Wang et al., 2025). This cardiotoxic liability curtails the widespread application of ATO, thereby necessitating the discovery of efficacious strategies to ameliorate its adverse cardiac effects, leveraging its anti-neoplastic attributes while preserving cardiac integrity—a quintessential challenge in clinical therapeutics.

Amygdalin (AMG), a cyanogenic glycoside also recognized as vitamin B17, is extracted from the mature seeds of the almond (*Prunus dulcis*), a member of the Rosaceae family. Its therapeutic repertoire is expansive, encompassing roles as an expectorant, antitussive, and adjunct in cancer chemotherapy (Liczbiński & Bukowska, 2018; Saleem, Asif, Asif, & Saleem, 2018). Compelling evidence suggests a synergistic impact of AMG with exercise on cardiac function, attenuating inflammation and fibrosis subsequent to myocardial infarction (Guo et al., 2024). Kung's research implicates the anti-inflammatory and antioxidant mechanisms of AMG in the amelioration of angiotensin II-induced cardiac hypertrophy, underscoring its protective potential (Kung et al., 2021). Prior studies have accentuated the cardioprotective attributes of AMG, attributed to its anti-inflammatory and antioxidant mechanisms (Guo et

al., 2025; Wang et al., 2022). However, the protective efficacy of AMG against ATO-induced cardiotoxicity and the elucidation of its underlying mechanisms remain unexplored territories within the scientific literature, beckoning further investigation.

The heart, as the organ with the highest energy demand, is critically dependent on the efficiency of mitochondrial oxidative phosphorylation (Pohjoismäki & Goffart, 2017). Mitochondria, prevalent in cardiac tissue (Brown et al., 2017), are dual-edged swords, serving as the powerhouse of the cell while concurrently generating reactive oxygen species (ROS) (Xue et al., 2020). The unchecked proliferation of ROS is a cardinal feature in ATO-induced myocardial injury (Liang et al., 2020). The surge in ROS production perturbs the physiological equilibrium, precipitating oxidative stress (Curtin, Donovan, & Cotter, 2002) and escalating the expression of inflammatory mediators such as tumor necrosis factor- α (TNF- α), thereby intensifying inflammatory pathology (Deng et al., 2020; Jia et al., 2021; Qiao, Zhang, Liu, Xu, & Li, 2022). Hence, the preservation of cellular energy equilibrium is paramount for the sustenance of an organism's vitality.

Adenosine 5'-monophosphate-activated protein kinase (AMPK) is a sentinel energy sensor enzyme, pivotal in the maintenance of cellular energy equilibrium under stress (Li, Chen, Li, Huang, & Zhao, 2020). AMPK orchestrates the activation of peroxisome proliferator-activated receptor gamma coactivator 1-alpha (PGC-1 α) to foster mitochondrial biogenesis and modulates the expression of antioxidant enzymes, including catalase (CAT), superoxide dismutase (SOD), and glutathione (GSH), through the activation of NRF2 (Liu et al., 2021). Sirtuin 1 (SIRT1), an NAD⁺-dependent deacetylase, is instrumental in a myriad of biological processes, such as cellular metabolism, apoptosis, inflammation, and oxidative stress. AMPK modulates these pathways through the activation of SIRT1-associated mechanisms (Li et al., 2020; Tian et al., 2019). SIRT1, in turn, suppresses the transcription of pro-inflammatory genes by deacetylating nuclear factor-kappa B (NF- κ B), AP-1, and histones, thereby attenuating the activity of transcription factors and the transcription of inflammation-related genes (Song & Zhou, 2022). NF- κ B, a multi-subunit complex with p65 being a critical component, plays a significant role in the innate immune response (Shan et al., 2019). The p65 subunit is implicated in the induction of Bax aggregation and caspase-3 activation through the upregulation of IL-1 β , culminating in cellular demise (Zheng, Bian, Zhang, Ren, & Li, 2020).

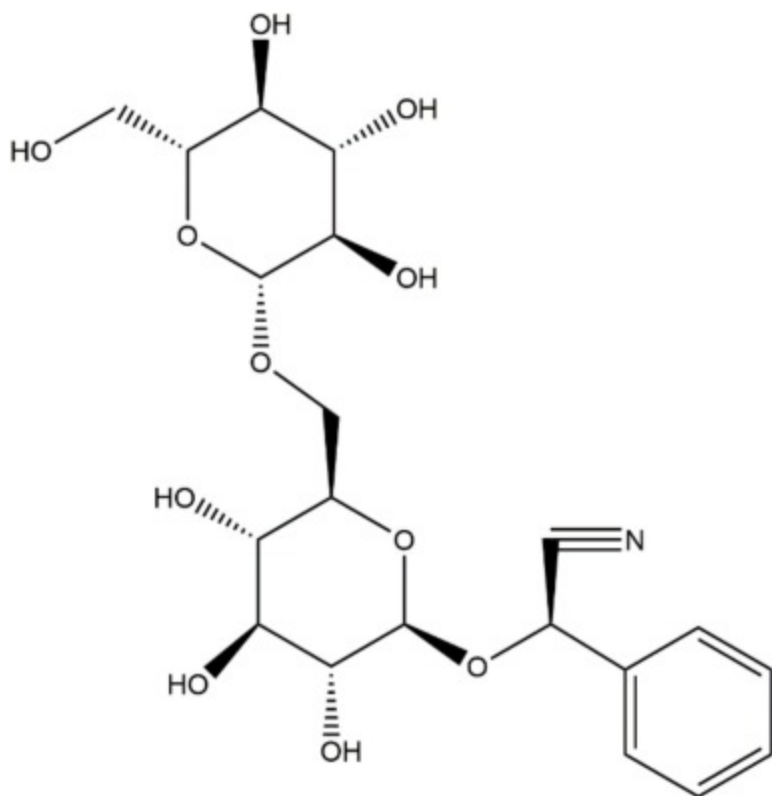
This study endeavors to construct a cardiotoxicity model in Sprague-Dawley (SD) rats through the administration of arsenic trioxide (ATO), aiming to delineate the protective effects of AMG against cardiotoxicity induced by ATO with a spotlight on oxidative stress, inflammation, and apoptosis. The underlying mechanism of this protective effect is

hypothesized to be associated with the activation of the AMPK/SIRT1 signaling pathway. Moreover, this investigation appraises the viability of employing AMG as a therapeutic intervention to mitigate cardiotoxicity associated with ATO in clinical scenarios.

2. Materials and methods

2.1. Reagents and solution preparation

Amygdalin (AMG) (Fig. 1), a biological reagent of 97% purity (Cat: S30650), was procured from Shanghai Yuanye Bio-Technology Co., Ltd. (Shanghai, China). Arsenic trioxide (ATO), with a certified purity exceeding 98%, was sourced from Shuanglu Pharmaceutical Co., Ltd. (Beijing, China). ATO was meticulously prepared by dissolving it in physiological saline, augmented with sodium hydroxide to facilitate dissolution. Subsequently, the pH of the ATO solution was finely adjusted to approximately neutral (pH7) using hydrochloric acid, aligning it with the physiological pH of the Sprague-Dawley rat's abdominal environment. In contrast, AMG was solubilized directly in deionized water for subsequent intragastric administration.



[Download: Download high-res image \(69KB\)](#)

[Download: Download full-size image](#)

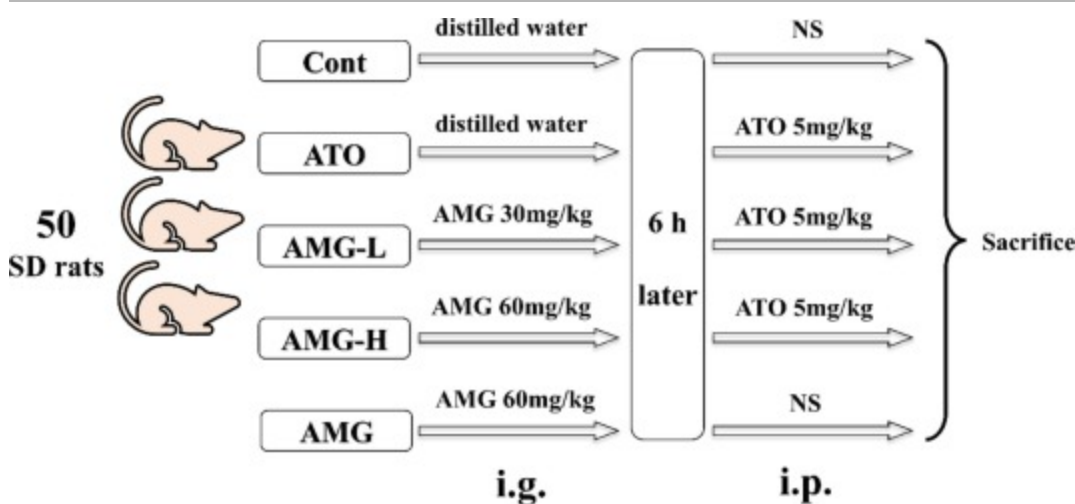
Fig. 1. Chemical structure of AMG.

2.2. Animal and ethical considerations

A cohort of fifty male Sprague-Dawley rats, each weighing 180 ± 10 g and fulfilling the specific pathogen-free (SPF) criteria. The animals were domiciled in our SPF-accredited animal experimental facility under a regimen of tightly controlled environmental conditions, including a temperature range of 21–23°C and humidity levels maintained between 55 and 58%. They were subjected to a 12-h light/dark cycle and provided with food and water ad libitum. The experimental protocols adhered to the stringent guidelines set forth by the Institutional Animal Ethical Committee of Hebei University of Chinese Medicine. The research design was sanctioned by the Animal Ethics Committee, with the assigned ethics approval number DWLL202307007.

2.3. Animal experimentation

Following an initial week of acclimatization to a standard diet, the Sprague-Dawley rats were randomly allocated into five distinct experimental cohorts ($n=10$) as follows (Fig. 2):



[Download: Download high-res image \(159KB\)](#)

[Download: Download full-size image](#)

Fig. 2. Study flowchart.

- (A) the Control (Cont) group;
- (B) the Arsenic Trioxide (ATO) group;
- (C) the Low-Dose Amygdalin plus ATO (AMG-L) group;
- (D) the High-Dose Amygdalin plus ATO (AMG—H) group;
- (E) the Amygdalin (AMG) group.

AMG or distilled water was administered by gavage daily at 10a.m., and after 6h, an intraperitoneal injection of ATO or saline was performed for 15 days. Daily food and water intake was meticulously recorded, with body weight measurements taken every third day.

At the culmination of the treatment period, 24h subsequent to the final dose, the rats were subjected to anesthesia using sodium pentobarbital (40mg/kg). An electrocardiogram (ECG) was conducted on the anesthetized rats to assess cardiac function. Subsequently, blood was extracted via exsanguination from the abdominal aorta, and serum was isolated by centrifugation at $1500\times g$ for 10min at 4°C , then stored at -20°C for subsequent analysis. The rats were then euthanized, and their hearts were expeditiously excised. The cardiac tissues were sectioned and fixed in either 10% neutral formalin or 2.5% glutaraldehyde phosphate buffer. The remaining tissue samples were either flash-frozen in liquid nitrogen or stored at -80°C for deferred biochemical assays.

2.4. Electrocardiogram recording and analysis

Post-treatment, the rats underwent a 12-h fast, devoid of food and water. Under anesthesia, three needle electrodes were strategically placed on the rats' forelimbs and hindlimb. ECG tracings were captured using the RM6240BD Biological Signal Collection system (Cheng Yi) to monitor alterations in the QT interval of the ECG. Bazett's formula, $QTc = QT/\sqrt{RR}$ (where RR denotes the rat's respiratory rate), was applied to correct the QT interval.

2.5. Echocardiography

Echocardiographic assessment of cardiac functionality was performed utilizing a high-resolution ultrasound imaging system equipped with an MS-250 probe (Vevo 2100, Visualsonics Inc., Toronto, Canada). Following the application of a couplant to the prepared skin area, the probe was maneuvered to acquire parasternal long-axis images of the left ventricle in two-dimensional B-mode. Cardiac performance was quantified by measuring the ejection fraction (EF), fractional shortening (FS), left ventricular end-systolic volume (LVESV), and left ventricular end-diastolic volume (LVEDV) using M-mode recordings from the short-axis view.

2.6. Histopathological analysis

The excised cardiac tissues were processed by fixation in 10% neutral formaldehyde, followed by embedding in paraffin wax. Tissue sections of $5\mu\text{m}$ thickness were prepared and subjected to histological examination through hematoxylin-eosin (H&E) and Masson's

staining to evaluate myocardial structure and presence of fibrosis. And pathological changes were observed under an optical microscope (Leica DM4000B, Solms, Germany).

2.7. Serum biochemical analysis

Total serum levels were quantified for creatine kinase (CK) (Nanjing Jiancheng Biological Co., Ltd.; Cat: A032-1-1), lactate dehydrogenase (LDH) (Nanjing Jiancheng Biological Co., Ltd.; Cat: A020-1-2), and cardiac troponin I (cTnI) (Hua Ying Biological Engineering Institute, Beijing, China; Cat: HY-D0022). Alterations in these biomarkers are closely correlated with changes in cardiac function.

2.8. Assay of heart antioxidants

Heart tissue samples were weighed to prepare a 10% (w/v) buffered homogenate, which was centrifuged at 1000g for 10min at 4°C to obtain the supernatant. According to the manufacturer's instructions, the activities or contents of malondialdehyde (MDA) (Cat: A003-1-2), superoxide dismutase (SOD) (Cat: A001-3-2), reduced glutathione (GSH) (Cat: A006-2-1), and catalase (CAT) (Cat: A007-1-1) in the heart were measured using the appropriate commercial kits from Nanjing Jiancheng Biological Co., Ltd.

2.9. ROS expression

Fresh frozen tissue sections were thawed and incubated with dihydroethidium for 30min under dark conditions. Subsequently, the sections were washed three times with PBS (5min each time) and stained with 4',6-diamidino-2-phenylindole (DAPI) at room temperature for 10min in the dark. Following these steps, the sections were sealed and imaged, and the results were observed and analyzed using a Tecnai G2 Spirit transmission electron microscope (TEM; ZOOM-1 HC-1, Hitachi, Japan).

2.10. Inflammatory cytokine analysis

To assess the effect of AMG on cytokine production, serum levels of tumor necrosis factor- α (TNF- α) (Cat: ER1393), interleukin-1 β (IL-1 β) (Cat: ER1094), and interleukin-6 (IL-6) (Cat: ER0042) were measured using ELISA kits from Wuhan Fine Biotech Co., Ltd., China, following the manufacturer's instructions.

2.11. Mitochondrial ultrastructure analysis

Left ventricular muscle samples (1 mm³) were fixed in a 2.5% glutaraldehyde phosphate buffer, rinsed with phosphate buffer (0.1 M, pH7.4) at 4°C, and subsequently fixed in 1%

osmium tetroxide. The samples were dehydrated with acetone, embedded, sectioned, and stained with uranyl acetate and lead citrate. The ultrastructural observations and analyses were performed using a Tecnai G2 Spirit transmission electron microscope (TEM; ZOOM-1 HC-1, Hitachi, Japan).

2.12. Cell culture and treatment

The H9c2 cell line was obtained from the cell bank of the Chinese Academy of Sciences (Shanghai, China). The cells were cultured in Dulbecco's modified Eagle's medium (DMEM, Gibco, USA) supplemented with 10% fetal bovine serum (FBS, Gibco, USA) and 1% penicillin–streptomycin (PS, Biosharp, China) within a CO₂ incubator set at 5% CO₂ and 37°C with saturated humidity. The cells were assigned to 5 groups: (A) Cont, the cells were cultured for 40h; (B) ATO, the cells were cultured for 16h and then treated with 10μM ATO (Wu et al., 2022; Zhang et al., 2018a) for 24h; (C) ATO+AMG, the cells were cultured for 4h and then treated with 320μM AMG (Kung et al., 2021) for 12h and finally treated with 10μM ATO for 24h; (D) ATO+CC(Compound C, an AMPK inhibitor), the cells were cultured for 12h and then treated with 10μM Compound C (Liu et al., 2022; Ye et al., 2020) for 4h and finally treated with 10μM ATO for 24h; (E) ATO+AMG+CC, the cells were treated with 10μM Compound C for 4h and then treated with 320μM AMG for 12h and finally treated with 10μM ATO for 24h.

2.13. Western blot analysis

Myocardial tissue was lysed in lysis buffer as per the manufacturer's protocol (Servicebio Co., Ltd., Wuhan, China) to extract total protein. Total protein (20μg per lane) was separated by 10% SDS-PAGE and transferred onto polyvinylidene fluoride membranes. The membranes were blocked with 5% skim milk buffer at 37°C for 2h and incubated overnight at 4°C with the following primary antibodies: anti-Bcl-2-associated X protein (Bax) (Servicebio, China; 1:1000; Cat: GB12690), anti-B-cell lymphoma-2 (Bcl-2) (Servicebio, China; 1:1000; Cat: GB124830), anti-Caspase-3 (Servicebio, China; 1:1000; Cat: GB11767C), anti-Cleaved-Caspase-3 (Servicebio, China; 1:1000; Cat: GB11767C), anti-AMPKα2 (Servicebio, China; 1:1000; Cat: GB112669), anti-p-AMPKα2 (CST, USA; 1:1000; Cat: 2535), anti-SIRT1 (Proteintech, USA; 1:1000; Cat: 13161-1-ap), anti-PGC-1α (Proteintech, USA; 1:1000; Cat: 66369-1-Ig), anti-NF-κB (p65) (Servicebio, China; 1:1000; Cat: GB12142), and anti-GAPDH (Servicebio, China; 1:2000; Cat: GB15002). Following primary antibody incubation, the membranes were washed with TBST three times (10min each) and incubated with horseradish peroxidase (HRP)-conjugated goat anti-rabbit IgG (Servicebio, China; 1:5000; Cat: GB23303) or HRP-conjugated goat anti-mouse IgG (Servicebio, China; 1:5000; Cat:

GB23301) at room temperature for 1 h. After three additional washes with TBST, protein bands were visualized and their grayscale values analyzed using ImageJ software.

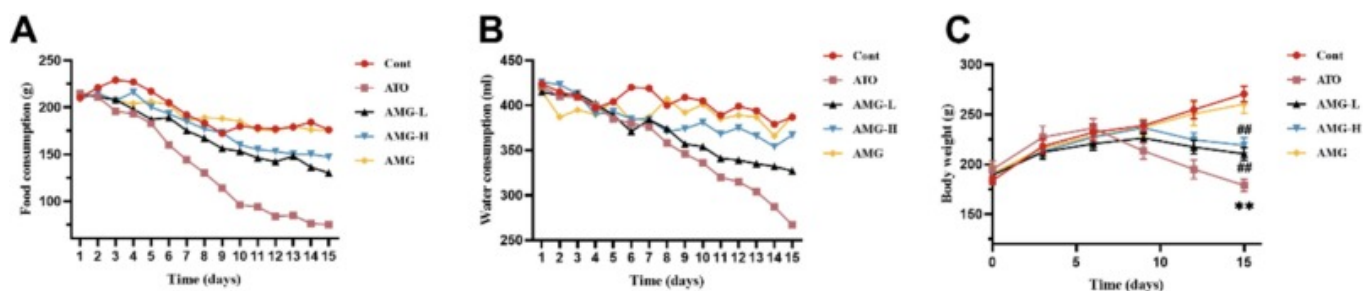
2.14. Statistical analysis

Data were subjected to rigorous analysis utilizing SPSS 26.0 software (SPSS Corporation), with results articulated as mean \pm standard deviation. To discern significant intergroup disparities, a one-way analysis of variance (ANOVA) complemented by Tukey's post hoc test was meticulously executed, establishing a threshold of significance at $P < 0.05$.

3. Results

3.1. Effects of AMG on diet, water intake, and body weight in rats

Throughout the treatment phase, astute observations delineated a pronounced divergence in the quotidian consumption of water and diet between the ATO group and its Cont group counterpart ($P < 0.01$; Fig. 3). Concomitantly, the body weight index at the experimental terminus depicted a significant decrement in the ATO group relative to the Cont group ($P < 0.01$), an effect attenuated by AMG intervention. Notably, the augmentation of body weight index within the AMG-L and AMG-H groups was stark in comparison to the ATO group ($P < 0.01$).



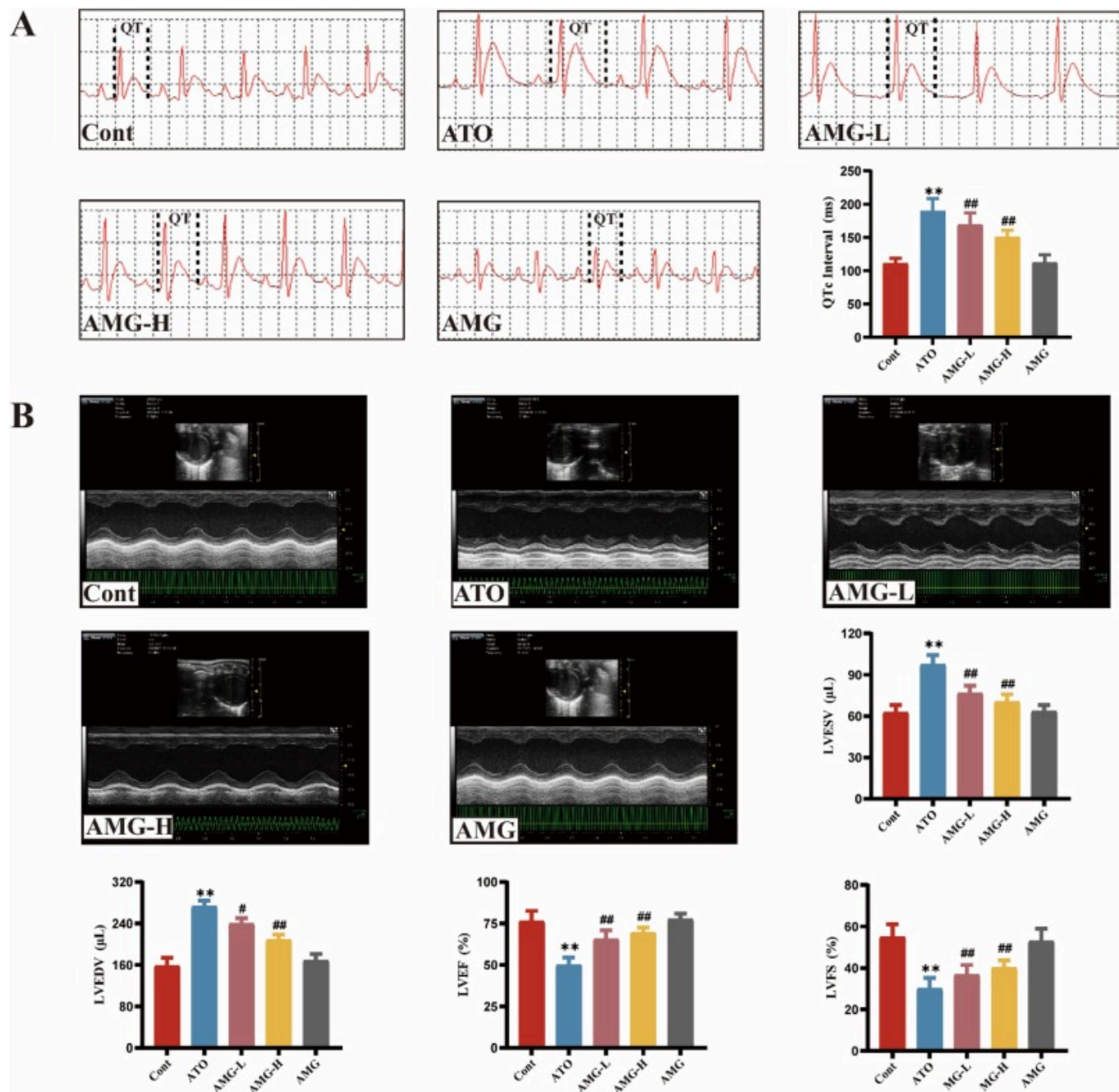
[Download: Download high-res image \(145KB\)](#)

[Download: Download full-size image](#)

Fig. 3. Graphical representation of the modulatory effects of AMG on dietary intake, water consumption, and corporal mass in rats. A: Linear chart delineating alterations in nutritional ingestion. B: Linear chart illustrating shifts in hydric consumption. C: Linear chart reflecting changes in somatic mass. Mean \pm SD ($n = 10$). ** $P < 0.01$ versus Cont group, ## $P < 0.01$ versus ATO group.

3.2. AMG ameliorates ECG and echocardiographic abnormalities in ATO-treated rats

Post-final treatment, ECG and echocardiographic assessments were conducted to evaluate the palliative influence of AMG on cardiac dysfunction induced by ATO. Prolongation of the QTc interval, a cardinal manifestation of ATO treatment, was conspicuously ameliorated by adjunctive AMG therapy. Isolated AMG administration did not elicit any perturbation in the QTc interval of the Control rats (Fig. 4A).



[Download: Download high-res image \(937KB\)](#)

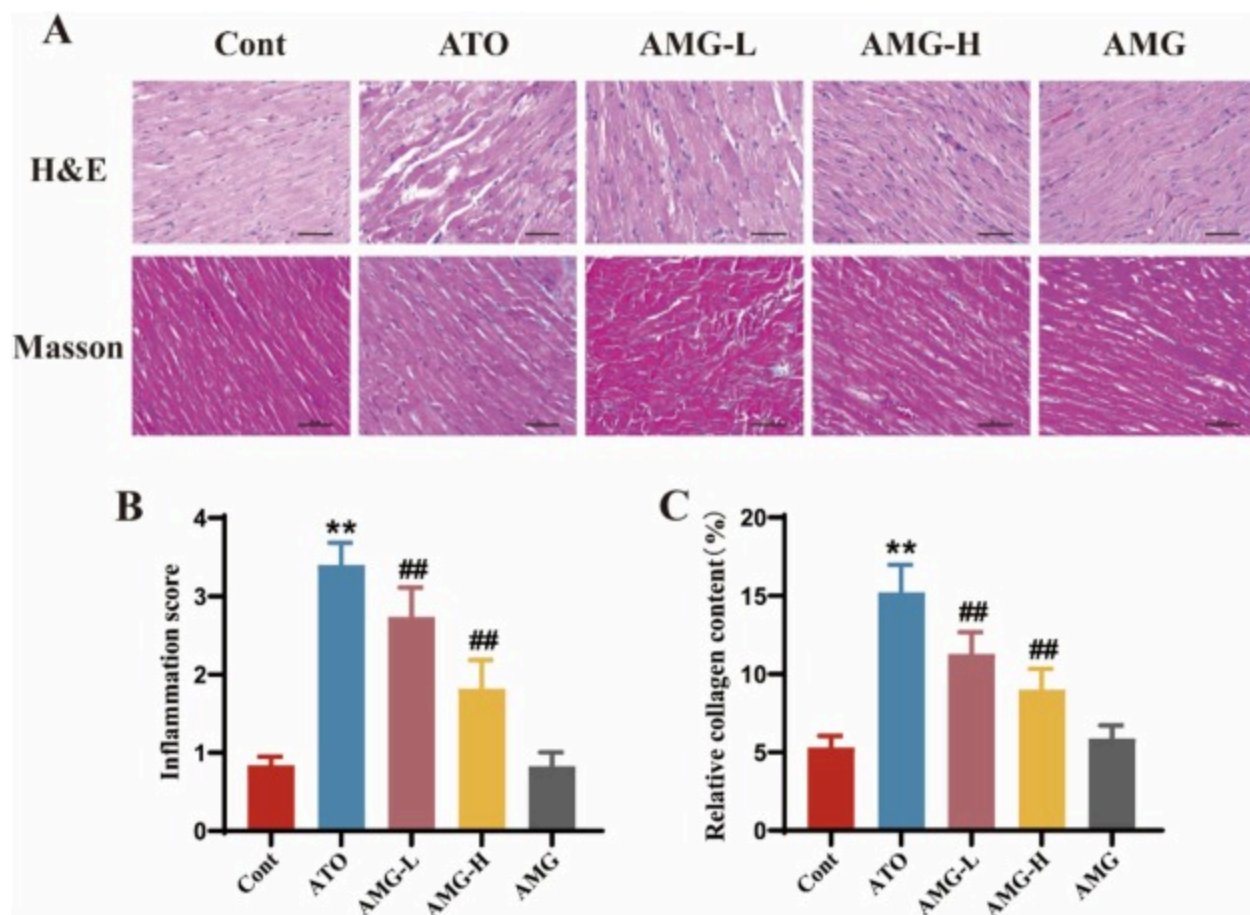
[Download: Download full-size image](#)

Fig. 4. AMG can ameliorate abnormal ECG and Echocardiographic caused by ATO. A: Changes of ECG waveforms after AMG treatment in rats. B: M-model echocardiography in rat. Mean±SD (n=10). **P<0.01 versus Cont group, #P<0.05, ##P<0.01 versus ATO group.

In juxtaposition to the Cont group, the ATO group exhibited exacerbated LVED and LVESV, concomitant with diminished LVEF and LVFS ($P < 0.01$), indicative of left ventricular dilation and compromised cardiac functionality. In stark contrast, the AMG-administered groups demonstrated a significant reduction in LVEDV and LVESV, alongside an enhancement in LVEF and LVFS ($P < 0.01$ or $P < 0.05$), underscoring the therapeutic efficacy of AMG, particularly at higher dosages (Fig. 4B).

3.3. Impact of AMG on ATO-elicited histopathological alterations

To quantitatively assess the cardioprotective effects of AMG on myocardial injury and fibrosis, histological examination employing H&E and Masson staining was performed on myocardial tissues. The Cont group displayed orderly arranged, structurally intact cardiomyocytes, whereas the ATO group exhibited cellular edema, eosinophilic cytoplasmic alterations, and conspicuous infiltration of inflammatory cells. Additionally, there was an evident deposition of collagen fibers between and around the blood vessels, with an intensified blue staining. Post-AMG treatment, a marked amelioration in cardiomyocyte morphology and collagen fiber arrangement was observed (Fig. 5).



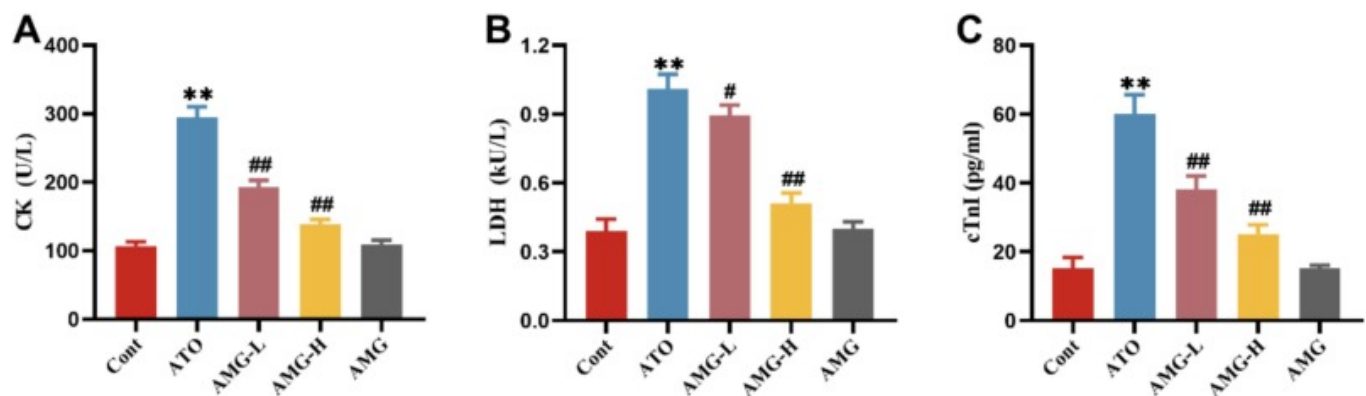
Download: [Download high-res image \(536KB\)](#)

Download: [Download full-size image](#)

Fig. 5. The effects of AMG on the cardiac histology in the rat were determined by H&E and Masson staining (200×, scale bar=50µm). A total of 10 photo fields from 5 animals were included in the semiquantitative analyses, which were conducted based on the inflammation score, the proportion of positive area for collagen fibrils. Data displayed as Mean±SD ($n=10$). ** $P<0.01$ versus Cont group, ## $P<0.01$ versus ATO group.

3.4. Influence of AMG on myocardial enzyme variations induced by ATO

Serum biomarkers of cardiac injury, namely CK, LDH, and cTnI, were quantified and exhibited significantly elevated levels in the ATO group when juxtaposed with the Cont group ($P<0.01$). Within the AMG-L and AMG-H groups, a discernible downward trend in these biomarkers was observed, in stark contrast to the ATO group ($P<0.05$ or $P<0.01$; Fig. 6).



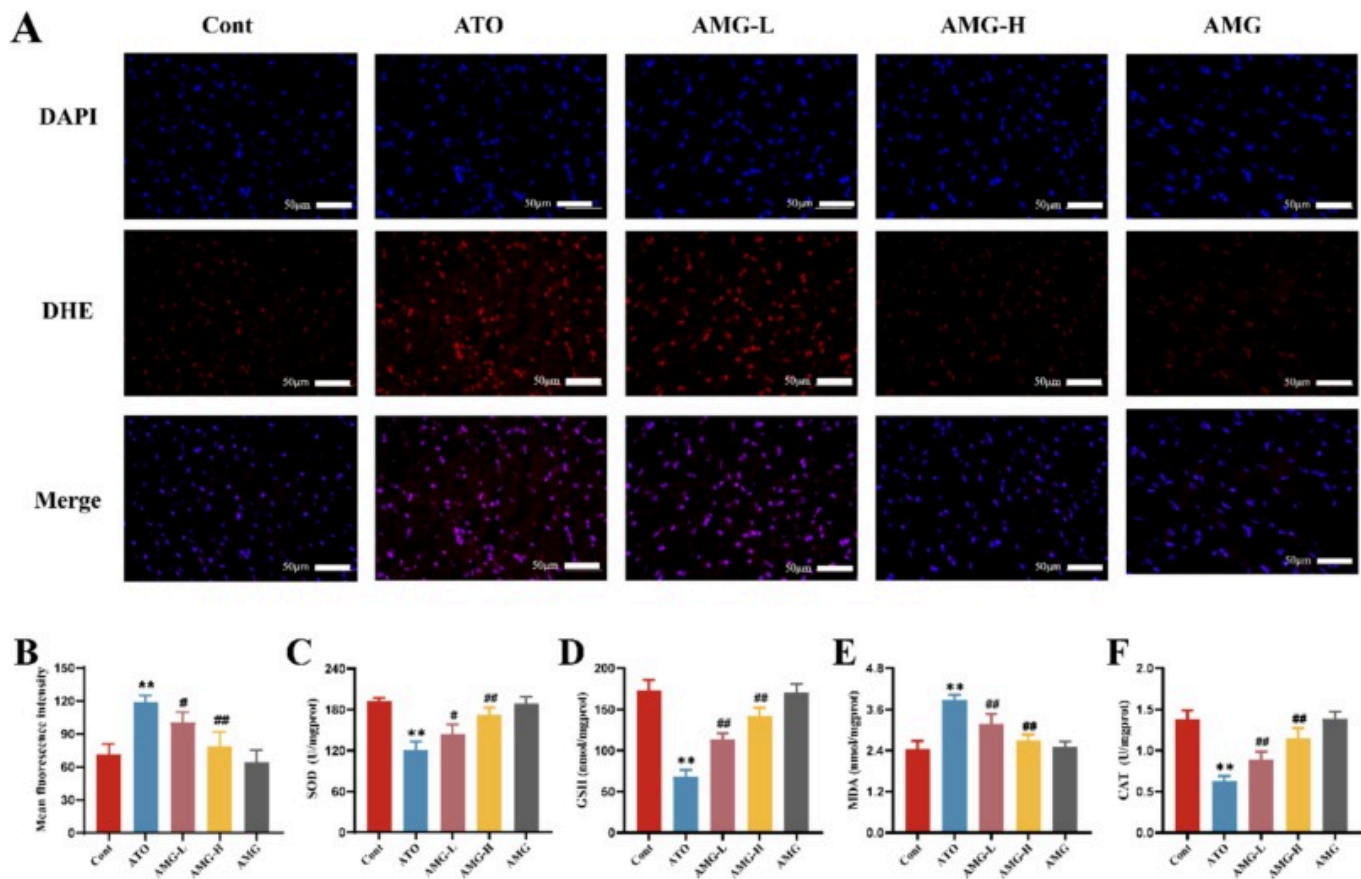
[Download: Download high-res image \(134KB\)](#)

[Download: Download full-size image](#)

Fig. 6. AMG can reduce the increased activities of CK (A), LDH (B) and cTnI(C) in serum caused by ATO. Mean±SD ($n=10$). ** $P<0.01$ versus Cont group, # $P<0.05$, ## $P<0.01$ versus ATO group.

3.5. Effects of AMG on oxidative stress in the heart

Myocardial damage was assessed by evaluating ROS in the frozen sections, as depicted in Fig. 7A. The fluorescence intensity of ROS in the ATO group was significantly increased compared to the Cont group. However, AMG-L and AMG-H treatments effectively suppressed the ATO-induced overexpression of ROS.



[Download: Download high-res image \(513KB\)](#)

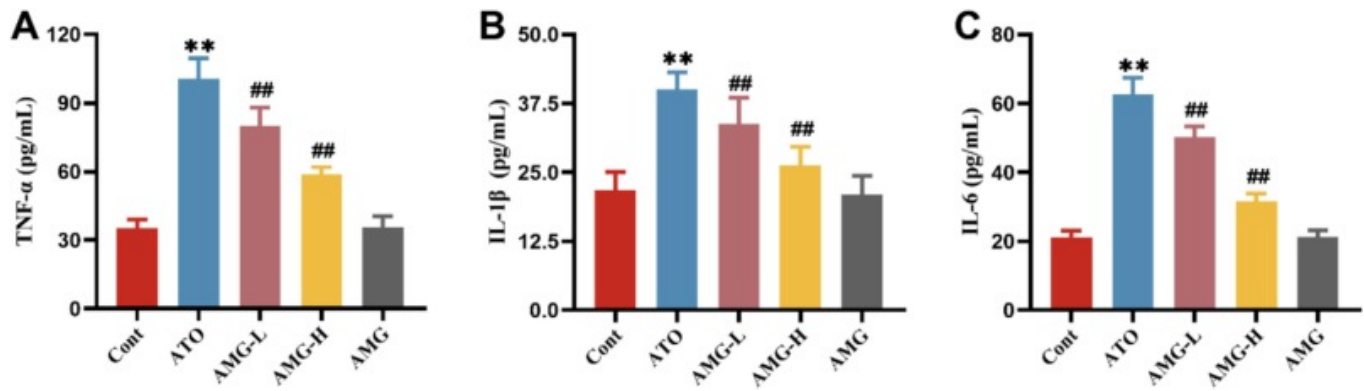
[Download: Download full-size image](#)

Fig. 7. A: AMG can attenuate ROS (B) overproduction in heart caused by ATO. AMG can ameliorate the variational activities of SOD (C), GSH (D), MDA (E) and CAT (F) in serum caused by ATO. Mean \pm SD ($n=10$). ** $P<0.01$ versus Cont group, # $P<0.05$, ## $P<0.01$ versus ATO group.

As shown in Figs. 7C-F, the tissue homogenate levels of SOD, GSH, MDA, and CAT were measured to assess oxidative stress activity. In the ATO group, there was a significant decrease in SOD (Fig. 7C), GSH (Fig. 7D), and CAT (Fig. 7F) levels, alongside an increase in MDA content (Fig. 7E), compared to the Cont group ($P<0.01$). Conversely, AMG-L and AMG-H treatments resulted in significant increases in SOD, GSH, and CAT levels ($P<0.05$ or $P<0.01$), and a decrease in MDA content ($P<0.01$).

3.6. Effects of AMG on IL-1 β , IL-6, and TNF- α

The results indicated that ATO induced a significant increase in the expression of inflammatory factors TNF- α , IL-1 β , and IL-6 compared with the Cont group ($P<0.01$). Notably, AMG treatment significantly down-regulated the levels of these inflammatory markers in a dose-dependent manner ($P<0.01$; Fig. 8).



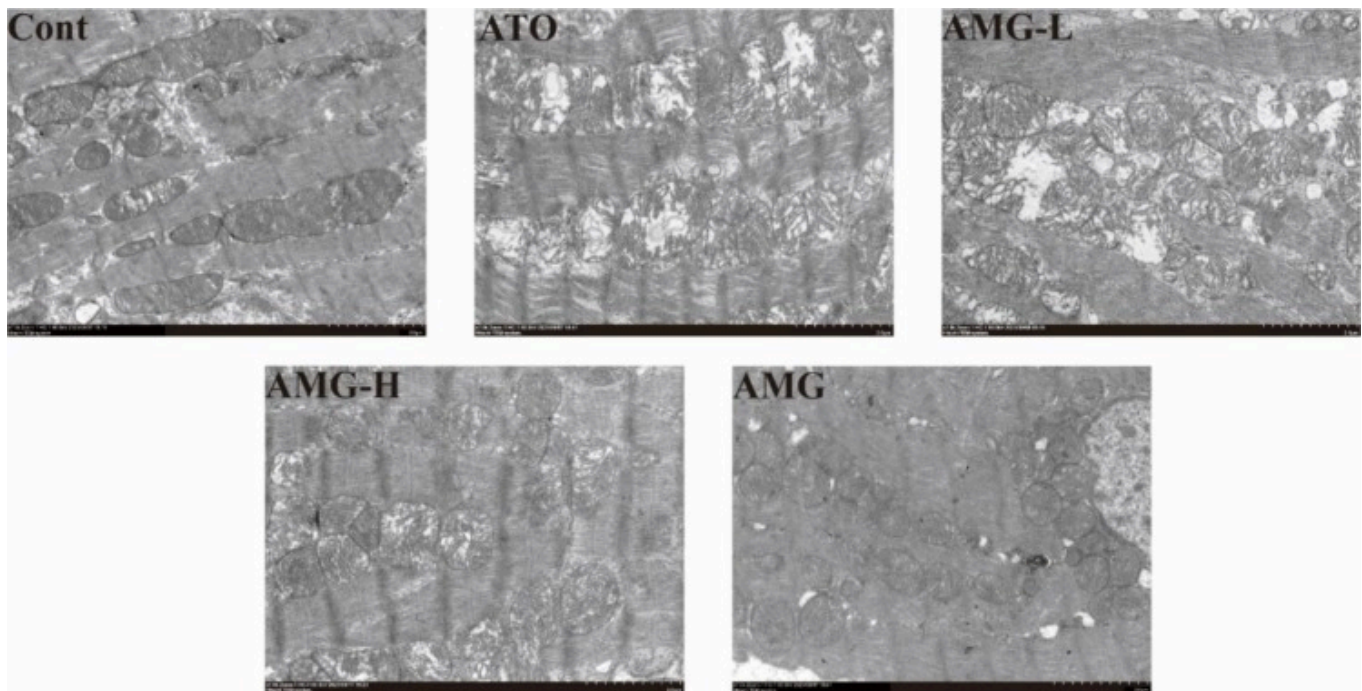
[Download: Download high-res image \(144KB\)](#)

[Download: Download full-size image](#)

Fig. 8. AMG can reduce the increased levels of inflammatory cytokines: TNF- α (A), IL-1 β (B) and IL-6 (C) in heart caused by ATO. Mean \pm SD (n=10). ** P <0.01 versus Cont group, ## P <0.01 versus ATO group.

3.7. Effects of AMG on ATO-induced changes in myocardial mitochondrial ultrastructure

Fig. 9 illustrates the ultrastructural changes in myocardial mitochondria across different treatment groups. In the Cont group, myocardial mitochondria displayed a normal morphological structure. However, myocardial tissue sections from the ATO group exhibited mitochondrial swelling, misaligned myofibrils and Z lines, reduced cristae, vacuolization, and significant disruption of membrane integrity. AMG-L and AMG-H treatments markedly improved mitochondrial ultrastructure, as evidenced by the absence of vacuolization and mitochondrial swelling compared to the ATO group.



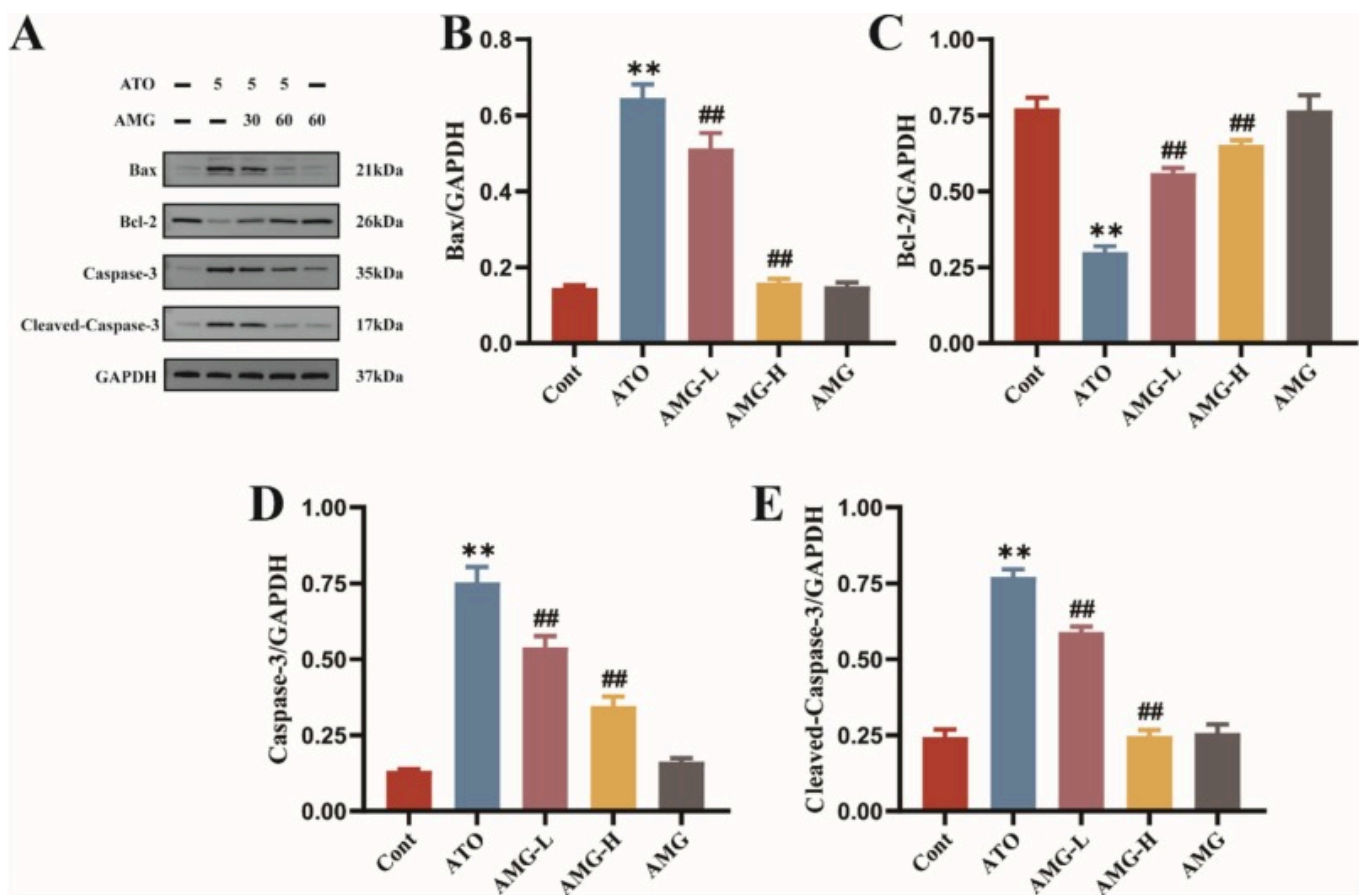
[Download: Download high-res image \(280KB\)](#)

[Download: Download full-size image](#)

Fig. 9. AMG can ameliorate the mitochondrial damage caused by ATO. Representative photomicrographs of mitochondria ultrastructural sections (6000 \times , scale bar=2 μ m).

3.8. Effects of AMG on ATO-induced changes in apoptosis

As shown in Fig. 10, western blot analysis of apoptosis-related proteins revealed a significant decrease in Bcl-2 expression, alongside up-regulated expressions of Bax, Caspase-3, and Cleaved-Caspase-3 in the ATO group compared to the Cont group ($P<0.01$). However, AMG treatment significantly enhanced Bcl-2 expression ($P<0.01$ or $P<0.05$) and reduced the expression of pro-apoptotic proteins (Bax, Caspase-3, and Cleaved-Caspase-3) ($P<0.05$ or $P<0.01$) compared to the ATO group.



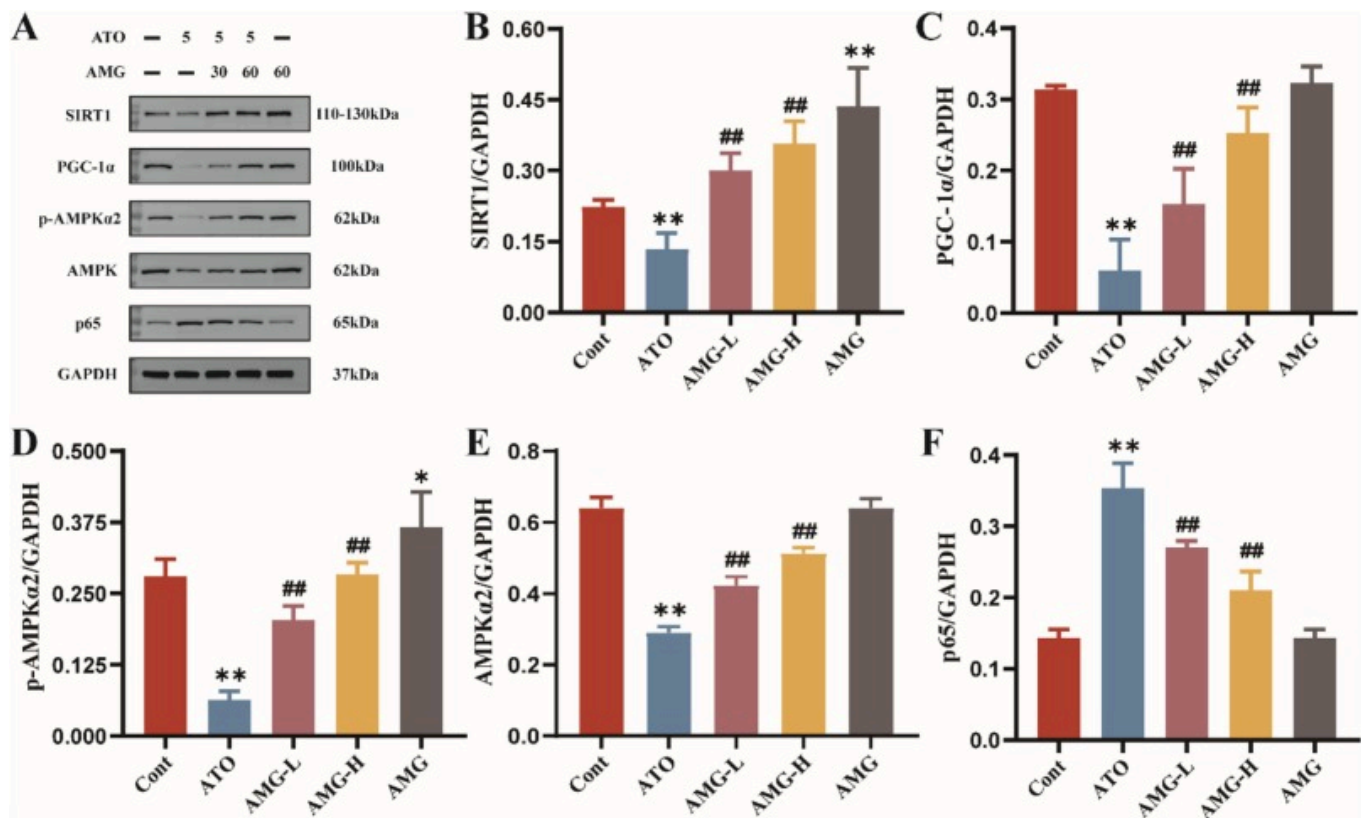
Download: [Download high-res image \(243KB\)](#)

Download: [Download full-size image](#)

Fig. 10. AMG can ameliorate the variational levels of apoptotic markers: Bax (B), Bcl-2 (C), Caspase-3 (D) and Cleaved-Caspase-3 (E) in heart caused by ATO. Mean \pm SD ($n=3$). ** $P<0.01$ versus Cont group, ## $P<0.01$ versus ATO group.

3.9. Effects of AMG on ATO-induced changes in p-AMPK α 2, AMPK, SIRT1, PGC1 α , and p65 expression

As shown in Fig. 11, western blot analysis of pathway-related proteins demonstrated a significant increase in NF- κ B (p65) levels and a marked decrease in p-AMPK α 2, AMPK α 2, SIRT1, and PGC-1 α levels in the ATO group compared to the Cont group ($P<0.01$). Conversely, AMG-L and AMG-H treatments up-regulated the expression of p-AMPK α 2, SIRT1, and PGC-1 α proteins, while down-regulating the expression of NF- κ B (p65) ($P<0.05$ or $P<0.01$).



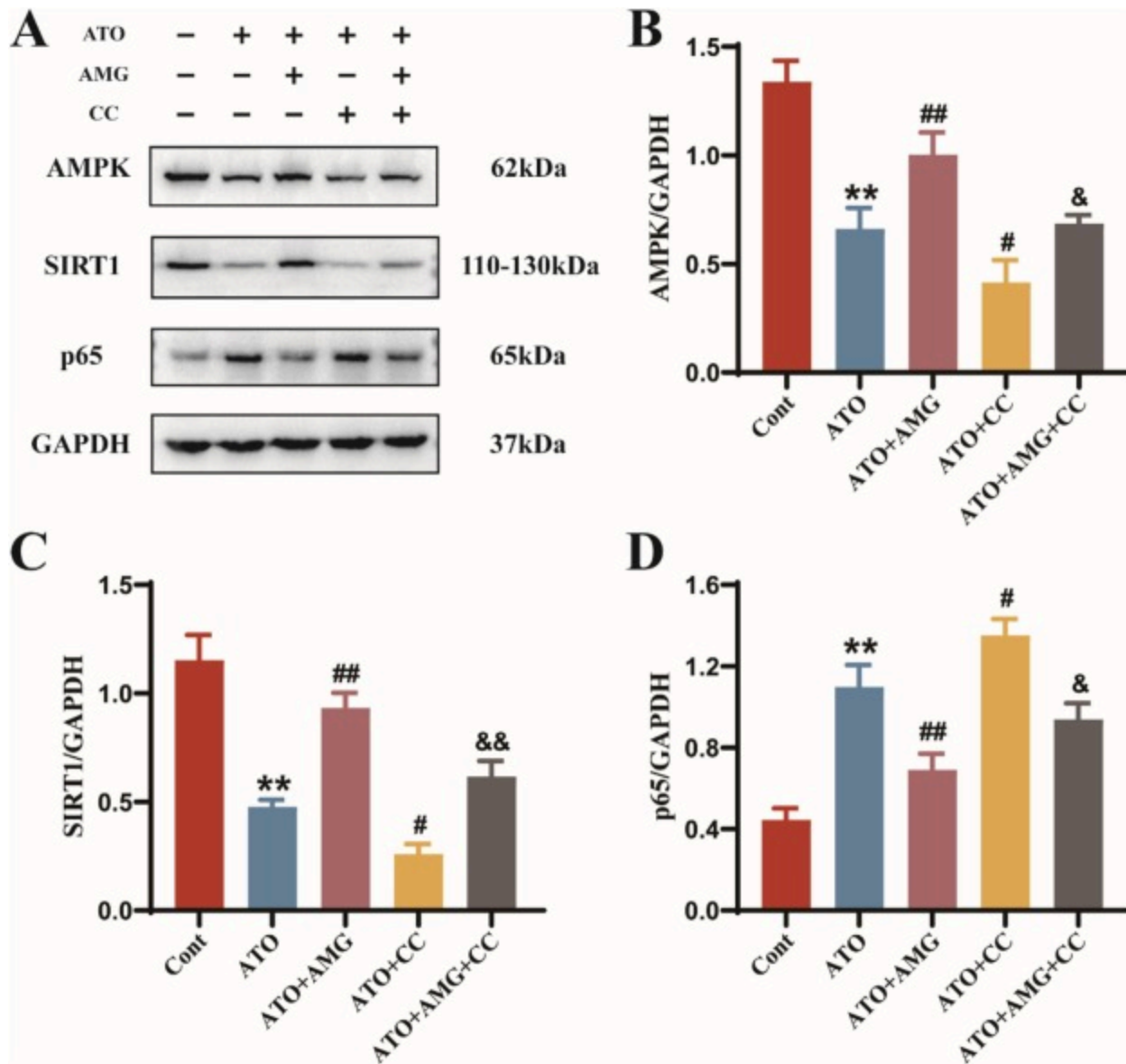
[Download: Download high-res image \(278KB\)](#)

[Download: Download full-size image](#)

Fig. 11. AMG can inhibit the activation of AMPK/SIRT1/PGC-1α pathway caused by ATO. Mean±SD (n=3). * $P<0.05$, ** $P<0.01$ versus Cont group, ## $P<0.01$ versus ATO group.

3.10. Effect of AMG combined with AMPK inhibitor on the expression of AMPK, SIRT1 and p65 in H9c2 cardiomyocytes stimulated by ATO

We hypothesize that AMG inhibits inflammatory responses by activating the AMPK signaling pathway, thereby protecting against ATO-induced cardiac toxicity. The results revealed that, compared with the Cont group, AMPK and SIRT1 expression levels in ATO group were significantly decreased ($P<0.01$), the p65 was increased ($P<0.01$). However, AMPK and SIRT1 expression levels were significantly increased ($P<0.01$), and p65 was significantly decreased ($P<0.01$) after AMG pretreatment. In addition, AMPK was significantly reduced ($P<0.05$) after the addition of AMPK inhibitor CC. Meanwhile, compared to ATO+AMG group, SIRT1 decreased ($P<0.01$), p65 increased ($P<0.05$) in ATO+AMG+CC group (Fig. 12). This study suggests that AMG inhibits cardiac toxicity by AMPK signaling pathway and that AMPK inhibitor CC can block this inhibition.



[Download: Download high-res image \(244KB\)](#)

[Download: Download full-size image](#)

Fig. 12. AMPK inhibitor CC abrogates inflammatory responses inhibiting effects of AMG. Mean \pm SD ($n=3$). ** $P<0.01$ versus Cont group, # $P<0.05$, ## $P<0.01$ versus ATO group, & $P<0.05$, && $P<0.01$ versus ATO+AMG group.

4. Discussion

ATO stands as an efficacious therapeutic agent in the treatment of APL and various malignancies. However, the clinical utility of ATO is significantly circumscribed by its profound cardiotoxicity (Jiang et al., 2023). The advent of ATO combination therapies has emerged as a viable strategy in leukemia treatment, with an increasing repertoire of adjunctive agents being identified to enhance the efficacy of ATO while mitigating its toxic

effects (Zhang et al., 2018b). Notably, botanical products have demonstrated a synergistic potential to augment ATO's therapeutic index.

Amygdalin (AMG), a principal bioactive constituent of almonds and a naturally occurring compound, boasts a spectrum of pharmacological properties, including anti-inflammatory, antibacterial, antioxidant, and immunomodulatory activities (Barakat et al., 2022). Our study presents evidence that pretreatment with AMG ameliorates ATO-induced cardiac injury in rats by attenuating oxidative stress, inflammatory cytokines, and apoptotic pathways. Furthermore, in the present study, to evaluate the potential toxicity of AMG, we established a Cont group and an AMG group. Detailed comparative analyses between the two groups, including behavioral activities, body weight changes, and multiple physiological/biochemical parameters, demonstrated no statistically significant differences ($P > 0.05$). These results indicate that amygdalin administration alone caused no detectable adverse effects on the organisms, exhibiting high safety within the applied dosage range without apparent toxic reactions. This finding provides substantial experimental evidence for the clinical application and further investigation of amygdalin, laying a solid safety foundation for its development and utilization in related fields.

Left ventricular diastolic dysfunction, a hallmark of cardiotoxicity, can insidiously progress to irreversible congestive cardiomyopathy, chronic heart failure, and, in severe cases, death (Bai et al., 2017; Liu, Liu, Tang, & Du, 2023; Zhang et al., 2021). In this investigation, we induced cardiotoxicity in a rat model through intraperitoneal ATO injection, followed by intervention with AMG. The findings revealed that ATO significantly diminished LVEF and LVFS, while augmenting LVEDD and LVESD compared to the Control group. These physiological manifestations, coupled with observed reductions in body weight, food consumption, and water intake, corroborate the detrimental impact on the rats' physiological performance (Fig. 3). Histopathological examination via H&E and Masson's trichrome staining unveiled pronounced pathological alterations in the ATO group, encompassing myocardial inflammatory cell infiltration, increased collagen deposition, and myocardial necrosis (Fig. 5). These observations allude to cardiac remodeling and myocardial fibrosis, sequelae of ATO-induced cardiotoxicity (Hemmati et al., 2018). Furthermore, the elongation of the QT interval on ECGs, indicative of long QT syndrome (LQT), is a known precursor to life-threatening arrhythmias such as torsades de pointes (TdP) (Li et al., 2022; Lu, Wang, Han, & Li, 2023). Our results corroborate the prolongation of the QTc interval in ATO-exposed rats, underscoring the successful establishment of a cardiotoxicity model. In stark contrast, AMG treatment groups exhibited significant improvements, substantiating AMG's cardioprotective effects against ATO-induced injury. Additionally, serum levels of CK, LDH, and cTnI, pivotal biomarkers of myocardial injury,

were markedly elevated in the ATO group but were significantly reduced upon AMG treatment, suggesting a protective mechanism mediated by the attenuation of these myocardial biomarker release (Singh, Goel, & Kaur, 2011).

Oxidative stress, apoptosis, and inflammation (Zhang et al., 2021) induced by ATO in living organisms significantly limit its clinical utility in cancer therapy. Oxidative impairment following ATO exposure is evidenced by decreased levels of SOD, CAT, and GSH, alongside increased levels of ROS and MDA (Abdel-Wahab, El-Shoura, Shafiuddin Habeeb, & Zafaar, 2023; Yang et al., 2019). These findings are consistent with our observations. Oxidative stress results in the generation of a substantial amount of ROS, which induces cellular injury by depleting antioxidant defenses and disrupting protein formation (Mandlik, Mandlik, & Patel, 2021). ROS can damage lipids and trigger the production of MDA, an unsaturated aldehyde produced by the oxidation of polyunsaturated fatty acids (Hu, Lei, Zhang, & Luo, 2022). SOD and CAT are key enzymes in the endogenous antioxidant system, constituting the first line of defense against oxidative damage. GSH, a non-enzymatic antioxidant, also plays a crucial role in clearing ROS (Zheng et al., 2013). SOD, CAT, GSH, and MDA serve as *in vivo* markers of oxidative stress. In this experiment, AMG treatment mitigated oxidative stress by enhancing the activities of SOD, CAT, and GSH, and reducing MDA levels (Fig. 7), thereby bolstering antioxidant defenses in the liver of ATO-intoxicated rats.

ATO is recognized as a mitochondrial toxin (Kumar, Yedjou, & Tchounwou, 2014), capable of inducing DNA damage/mutation and causing mitotic arrest and apoptosis by altering mitochondrial membrane potential (Cai et al., 2003; Finsterer & Ohnsorge, 2013). This phenomenon was corroborated by experimental results (Fig. 9), which revealed abnormalities in mitochondrial ultrastructure observed by TEM in the hearts of ATO-intoxicated rats. It is postulated that ATO-induced disruption of ROS balance is related to mitochondrial dysfunction. Arsenic toxicity can impair the mitochondrial electron transfer chain, leading to decreased ATP production, inhibited mitochondrial transmembrane potential, and increased mitochondrial ROS production (Te Lintel et al., 2021), exacerbating myocardial damage.

Numerous studies suggest a bidirectional relationship between mitochondrial dysfunction, ROS, and chronic inflammatory diseases (Faas & de Vos, 2020). Mitochondrial dysfunctions have been identified in various autoimmune diseases (Haneklaus & O'Neill, 2015), with elevated expression of pro-inflammatory cytokines such as TNF- α , IL-6, and IL-1 β in affected patients (Zhang, Zhang, Wang, Li, & Zhang, 2018). Inflammation plays a crucial role in the pathogenesis of ATO-induced cardiotoxicity (Liang et al., 2020), with inflammatory cells (including neutrophils and mononuclear macrophages) and cytokines like TNF- α and IL-6

being essential components of the inflammatory response (Liu et al., 2020). ROS-activated macrophages and neutrophils can stimulate the upregulation of TNF- α , IL-1 β , and IL-6 expression (Pei, Wen, Cui, Yang, & Xie, 2021). TNF- α , a key proinflammatory cytokine, enhances the expression of various proinflammatory factor genes, including IL-6, thereby intensifying the inflammatory response (Wang et al., 2022). IL-1 β , a prominent member of the interleukin family, activates neutrophils to release proinflammatory mediators and has emerged as a promising target for potential cardiovascular disease treatments (Liu et al., 2022). AMG has been shown to diminish the levels of IL-6 and TNF- α , thereby exerting an anti-inflammatory effect and enhancing the immune response.

Mitochondria are cellular organelles responsible for producing the majority of ATP through oxidative phosphorylation (An et al., 2021). Excessive ROS levels, a byproduct of oxidative phosphorylation, are a significant factor in inducing apoptosis (Liu et al., 2021), with the Bcl-2 family serving as key regulators of mitochondrial apoptosis. Cellular stress activates the Bcl-2 family of proteins, leading to mitochondrial membrane permeabilization and the release of pro-apoptotic proteins like Bax (Cheng, Leach, & Hardwick, 2008). This results in the formation of the apoptosome, which activates caspase-3 and initiates apoptosis (Su et al., 2019). Our research observed that ATO-induced apoptosis was accompanied by increased intracellular ROS levels, suggesting that the mitochondrial pathway may be primarily responsible for this effect. Western blot analysis revealed that ATO exposure elevated levels of Bax and Cleaved-caspase-3 while decreasing Bcl-2 expression. Conversely, AMG exerted a suppressive effect on these changes. Our findings demonstrate that amygdalin attenuates ATO-induced myocardial apoptosis, potentially through its regulatory influence on the Bcl-2/Bax signaling cascade.

To delve deeper into the molecular underpinnings of AMG's ameliorative effects on ATO-induced mitochondrial dysfunction, this study employed western blot analysis to scrutinize pivotal components of the AMPK/SIRT1/PGC-1 α signaling cascade, integral to mitochondrial biogenesis (Gu et al., 2022). AMPK, an essential energy sensor, is pivotal in the regulation of cellular energy equilibrium and significantly contributes to cardiac energy metabolism (Koyani et al., 2020). Activation of AMPK augments SIRT1 activity, modulating intracellular NAD⁺ levels (Cantó et al., 2009). The interplay between AMPK and SIRT1, responsive to cellular energetic and redox status, modulates PGC-1 α activity through a combination of phosphorylation and deacetylation, respectively (Liu, Li, et al., 2021). PGC-1 α , a transcriptional coactivator prevalent in cardiac tissue (Thompson, Davison, Crawford, & Hughes, 2022), governs the expression of mitochondrial proteins implicated in oxidative stress regulation (Choi et al., 2017), thereby exerting protective effects against oxidative stress. Notably, AMPK activation has been shown to attenuate NF- κ B phosphorylation in

macrophages (Yang, Kahn, Shi, & Xue, 2010), with subsequent implications for the regulation of inflammatory responses through the AMPK/SIRT1/NF- κ B axis (Chen & Lan, 2017; Park et al., 2023; Wang et al., 2020).

Our investigation revealed that ATO treatment diminished the activity of the AMPK/SIRT1 pathway in cardiac tissue, culminating in heightened NF- κ B activation and the concomitant secretion of pro-inflammatory cytokines, including TNF- α , IL-1 β , and IL-6 (Ding et al., 2024). In stark contrast, AMG treatment precipitated a marked elevation in p-AMPK protein expression, effectively igniting the AMPK/SIRT1 pathway within ATO-challenged cardiac tissue and concurrently repressing NF- κ B expression. Moreover, the upregulation of the NF- κ B p65 subunit has been shown to dampen PGC-1 α promoter activity (Rabinovich-Nikitin, Blant, Dhingra, Kirshenbaum, & Czubryt, 2022), suggesting that interventions directed at NF- κ B signaling may safeguard PGC-1 α function and mitochondrial integrity amidst oxidative stress. Collectively, these observations suggest that AMG counteracts the ROS and inflammatory escalation incited by ATO, with the enhancement of mitochondrial function potentially attributable to the activation of the AMPK/SIRT1 pathway, thus curbing apoptosis and inflammation.

The findings of the current study also indicate that AMPK inhibitor CC inhibited SIRT1 upregulation and p65 downregulation in AMG-treated ATO-stimulated cardiomyocytes. These results suggest the importance of AMPK/SIRT1/p65 signaling pathway in the treatment of ATO-induced cardiotoxicity, and that AMG may enhance its signaling pathway to ameliorate ATO cardiotoxicity (Fig. 12).

In summation, AMG, esteemed as a beneficial dietary component or therapeutic agent, harbors the potential to ameliorate ATO-induced cardiac injury by quelling oxidative stress, apoptosis, and inflammation. The mechanisms underpinning this cardioprotective effect may be intricately linked to the activation of the AMPK/SIRT1 signaling pathway. The findings of this study shed further light on the molecular mechanisms through which AMG confers its beneficial impact on ATO-induced cardiac injury.

Authors' contribution

DM and HG contributed to the research design. OY and YW contributed to the experiments. KH and MZ contributed data analysis. DM, HW and YS contributed to manuscript writing and revising. All authors contributed to the article and approved the submitted version.

CRedit authorship contribution statement

Haochuan Guo: Writing – original draft, Visualization, Validation, Methodology, Investigation, Data curation. **Yanfei Ouyang:** Writing – original draft, Project administration, Methodology, Conceptualization. **Yuxia Wang:** Resources, Methodology, Investigation. **Keqian He:** Supervision, Software, Conceptualization. **Zhihong Ma:** Supervision, Software, Conceptualization. **Mengwei Zhao:** Validation, Supervision, Methodology. **Yongxing Song:** Writing – review & editing, Supervision, Funding acquisition, Data curation. **Hongfang Wang:** Writing – review & editing, Methodology, Investigation, Conceptualization. **Donglai Ma:** Writing – review & editing, Writing – original draft, Project administration, Funding acquisition, Formal analysis, Conceptualization.

Ethical statement

I certify that this manuscript is original and has not been published and will not be submitted elsewhere for publication while being considered by Journal of Functional Foods. And the study is not split up into several parts to increase the quantity of submissions and submitted to various journals or to one journal over time. No data have been fabricated or manipulated (including images) to support your conclusions. No data, text, or theories by others are presented as if they were our own.

The submission has been received explicitly from all co-authors. And authors whose names appear on the submission have contributed sufficiently to the scientific work and therefore share collective responsibility and accountability for the results.

Funding

This research was supported by the Natural Sciences Foundation of Hebei Province of China (No. H2022423297, H2021423034), the Administration of Traditional Chinese Medicine of Hebei Province of China (No. 2022366, 2023118) and Foundation of Hebei University of Chinese Medicine (No. YZZZ2023008).

Declaration of competing interest



The authors declare that they have no known competing financial interests or personal relationships that could have appeared to influence the work reported in this paper.



[Recommended articles](#)

Data availability

Data will be made available on request.

References

- [Abdel-Wahab, El-Shoura, Shafiuddin Habeeb and Zafaar, 2023](#) B.A. Abdel-Wahab, E.A.M. El-Shoura, M. Shafiuddin Habeeb, D. Zafaar
Febuxostat alleviates arsenic trioxide-induced renal injury in rats: Insights on the crosstalk between NLRP3/TLR4, Sirt-1/NF- κ B/TGF- β signaling pathways, and miR-23b-3p, miR-181a-5b expression
Biochemical Pharmacology, 216 (2023), Article 115794
 [View PDF](#) [View article](#) [View in Scopus ↗](#) [Google Scholar ↗](#)
- [An et al., 2021](#) R. An, X. Wang, L. Yang, J. Zhang, N. Wang, F. Xu, ..., L. Zhang
Polystyrene microplastics cause granulosa cells apoptosis and fibrosis in ovary through oxidative stress in rats
Toxicology, 449 (2021), Article 152665
 [View PDF](#) [View article](#) [View in Scopus ↗](#) [Google Scholar ↗](#)
- [Bai et al., 2017](#) Y. Bai, Q. Chen, Y.P. Sun, X. Wang, L. Lv, L.P. Zhang, ..., X.L. Wang
Sulforaphane protection against the development of doxorubicin-induced chronic heart failure is associated with Nrf2 upregulation
Cardiovascular Therapeutics, 35 (5) (2017)
[Google Scholar ↗](#)
- [Barakat et al., 2022](#) H. Barakat, T. Aljutaily, M.S. Almujaaydil, R.M. Algheshairy, R.M. Alhomaïd, A.S. Almutairi, ..., A.A.H. Abdellatif
Amygdalin: A review on its characteristics, antioxidant potential, gastrointestinal microbiota intervention, anticancer therapeutic and mechanisms, toxicity, and encapsulation
Biomolecules, 12 (10) (2022)
[Google Scholar ↗](#)
- [Brown et al., 2017](#) D.A. Brown, J.B. Perry, M.E. Allen, H.N. Sabbah, B.L. Stauffer, S.R. Shaikh, ..., A.A. Voors, *et al.*
Expert consensus document: Mitochondrial function as a therapeutic target in heart failure
Nature Reviews Cardiology, 14 (4) (2017), pp. 238-250
[Crossref ↗](#) [View in Scopus ↗](#) [Google Scholar ↗](#)

- [Cai et al., 2003](#) X. Cai, Y. Yu, Y. Huang, L. Zhang, P.M. Jia, Q. Zhao, ..., G.Q. Chen
Arsenic trioxide-induced mitotic arrest and apoptosis in acute promyelocytic leukemia cells
Leukemia, 17 (7) (2003), pp. 1333-1337
[Crossref ↗](#) [View in Scopus ↗](#) [Google Scholar ↗](#)
- [Cantó et al., 2009](#) C. Cantó, Z. Gerhart-Hines, J.N. Feige, M. Lagouge, L. Noriega, J.C. Milne, ..., J. Auwerx
AMPK regulates energy expenditure by modulating NAD⁺ metabolism and SIRT1 activity
Nature, 458 (7241) (2009), pp. 1056-1060
[Crossref ↗](#) [View in Scopus ↗](#) [Google Scholar ↗](#)
- [Chen and Lan, 2017](#) L. Chen, Z. Lan
Polydatin attenuates potassium oxonate-induced hyperuricemia and kidney inflammation by inhibiting NF- κ B/NLRP3 inflammasome activation via the AMPK/SIRT1 pathway
Food & Function, 8 (5) (2017), pp. 1785-1792
[View in Scopus ↗](#) [Google Scholar ↗](#)
- [Cheng, Leach and Hardwick, 2008](#) W.C. Cheng, K.M. Leach, J.M. Hardwick
Mitochondrial death pathways in yeast and mammalian cells
Biochimica et Biophysica Acta, 1783 (7) (2008), pp. 1272-1279
 [View PDF](#) [View article](#) [View in Scopus ↗](#) [Google Scholar ↗](#)
- [Choi et al., 2017](#) H.I. Choi, H.J. Kim, J.S. Park, I.J. Kim, E.H. Bae, S.K. Ma, S.W. Kim
PGC-1 α attenuates hydrogen peroxide-induced apoptotic cell death by upregulating Nrf-2 via GSK3 β inactivation mediated by activated p38 in HK-2 cells
Scientific Reports, 7 (1) (2017), p. 4319
[View in Scopus ↗](#) [Google Scholar ↗](#)
- [Curtin, Donovan and Cotter, 2002](#) J.F. Curtin, M. Donovan, T.G. Cotter
Regulation and measurement of oxidative stress in apoptosis
Journal of Immunological Methods, 265 (1) (2002), pp. 49-72
 [View PDF](#) [View article](#) [View in Scopus ↗](#) [Google Scholar ↗](#)
- [Deng et al., 2020](#) J.S. Deng, W.P. Jiang, C.C. Chen, L.Y. Lee, P.Y. Li, W.C. Huang, ..., G.J. Huang

Cordyceps cicadae mycelia ameliorate cisplatin-induced acute kidney injury by suppressing the TLR4/NF- κ B/MAPK and activating the HO-1/Nrf2 and Sirt-1/AMPK pathways in mice

Oxidative Medicine and Cellular Longevity, 2020 (2020), p. 7912763

[View in Scopus](#) [Google Scholar](#)

[Ding et al., 2024](#) M. Ding, C. Wang, J. Hu, J. She, R. Shi, Y. Liu, ..., W. Wu, *et al.*

PLOD3 facilitated T cell activation in the colorectal tumor microenvironment and liver metastasis by the TNF- α /NF- κ B pathway

Journal of Translational Medicine, 22 (1) (2024), p. 30

[View in Scopus](#) [Google Scholar](#)

[Faas and de Vos, 2020](#) M.M. Faas, P. de Vos

Mitochondrial function in immune cells in health and disease

Biochimica et biophysica acta Molecular basis of disease, 1866 (10) (2020), Article 165845

 [View PDF](#) [View article](#) [View in Scopus](#) [Google Scholar](#)

[Finsterer and Ohnsorge, 2013](#) J. Finsterer, P. Ohnsorge

Influence of mitochondrion-toxic agents on the cardiovascular system

Regulatory toxicology and pharmacology: RTP, 67 (3) (2013), pp. 434-445

 [View PDF](#) [View article](#) [View in Scopus](#) [Google Scholar](#)

[Fox et al., 2008](#) E. Fox, B.I. Razzouk, B.C. Widemann, S. Xiao, M. O'Brien, W. Goodspeed, ..., F.M. Balis, *et al.*

Phase 1 trial and pharmacokinetic study of arsenic trioxide in children and adolescents with refractory or relapsed acute leukemia, including acute promyelocytic leukemia or lymphoma

Blood, 111 (2) (2008), pp. 566-573

 [View PDF](#) [View article](#) [Crossref](#) [View in Scopus](#) [Google Scholar](#)

[Gu et al., 2022](#) M. Gu, Z. Wei, X. Wang, Y. Gao, D. Wang, X. Liu, ..., G. Li

Myostatin knockout affects mitochondrial function by inhibiting the AMPK/SIRT1/PGC-1 α pathway in skeletal muscle

International Journal of Molecular Sciences, 23 (22) (2022)

[Google Scholar](#)

[Guo et al., 2023](#) X. Guo, F.X. Qu, J.D. Zhang, F. Zheng, Y. Xin, R. Wang, ..., C.H. Lu

Amygdalin and exercise training exert a synergistic effect in improving cardiac performance and ameliorating cardiac inflammation and fibrosis in

a rat model of myocardial infarction. *Applied physiology, nutrition, and metabolism = Physiologie appliquee, nutrition et metabolisme*

(2023)

[Google Scholar ↗](#)

[Guo et al., 2024](#) X. Guo, F.X. Qu, J.D. Zhang, F. Zheng, Y. Xin, R. Wang, ..., C.H. Lu

Amygdalin and exercise training exert a synergistic effect in improving cardiac performance and ameliorating cardiac inflammation and fibrosis in a rat model of myocardial infarction

Applied physiology, nutrition, and metabolism Physiologie appliquee, nutrition et metabolisme, 49 (3) (2024), pp. 360-374

[Crossref ↗](#) [View in Scopus ↗](#) [Google Scholar ↗](#)

[Haneklaus and O'Neill, 2015](#) M. Haneklaus, L.A. O'Neill

NLRP3 at the interface of metabolism and inflammation

Immunological Reviews, 265 (1) (2015), pp. 53-62

[Crossref ↗](#) [View in Scopus ↗](#) [Google Scholar ↗](#)

[Hemmati et al., 2018](#) A.A. Hemmati, S. Olapour, H.N. Varzi, M.J. Khodayar, M. Dianat, B.

Mohammadian, H. Yaghooti

Ellagic acid protects against arsenic trioxide-induced cardiotoxicity in rat

Human & Experimental Toxicology, 37 (4) (2018), pp. 412-419

[Crossref ↗](#) [View in Scopus ↗](#) [Google Scholar ↗](#)

[Hofmann et al., 2020](#) S. Hofmann, J.L. Mai, S. Masser, P. Groitl, A. Herrmann, T. Sternsdorf, ..., S. Schreiner

ATO (arsenic trioxide) effects on Promyelocytic leukemia nuclear bodies reveals antiviral intervention capacity

Advancement of Science, 7 (8) (2020)

[Google Scholar ↗](#)

[Hu, Lei, Zhang and Luo, 2022](#) H.C. Hu, Y.H. Lei, W.H. Zhang, X.Q. Luo

Antioxidant and anti-inflammatory properties of resveratrol in diabetic nephropathy: A systematic review and Meta-analysis of animal studies

Frontiers in Pharmacology, 13 (2022), Article 841818

[View in Scopus ↗](#) [Google Scholar ↗](#)

[Jia et al., 2021](#) Y. Jia, J. Li, P. Liu, M. Si, Y. Jin, H. Wang, ..., L. Chu

Based on activation of p62-Keap1-Nrf2 pathway, hesperidin protects arsenic-trioxide-induced cardiotoxicity in mice

Frontiers in Pharmacology, 12 (2021), Article 758670

[View in Scopus ↗](#) [Google Scholar ↗](#)

[Jiang et al., 2023](#) Y. Jiang, X. Shen, F. Zhi, Z. Wen, Y. Gao, J. Xu, ..., Y. Bai

An overview of arsenic trioxide-involved combined treatment algorithms for leukemia: Basic concepts and clinical implications

Cell Death Discovery, 9 (1) (2023), p. 266

[Crossref ↗](#) [Google Scholar ↗](#)

[Koyani et al., 2020](#) C.N. Koyani, I. Plastira, H. Sourij, S. Hallström, A. Schmidt, P.P. Rainer, ..., D. von Lewinski

Empagliflozin protects heart from inflammation and energy depletion via AMPK activation

Pharmacological Research, 158 (2020), Article 104870

 [View PDF](#) [View article](#) [View in Scopus ↗](#) [Google Scholar ↗](#)

[Kumar, Yedjou and Tchounwou, 2014](#) S. Kumar, C.G. Yedjou, P.B. Tchounwou

Arsenic trioxide induces oxidative stress, DNA damage, and mitochondrial pathway of apoptosis in human leukemia (HL-60) cells

Journal of experimental & clinical cancer research: CR, 33 (1) (2014), p. 42

[Crossref ↗](#) [Google Scholar ↗](#)

[Kung et al., 2021](#) Y.L. Kung, C.Y. Lu, K.F. Badrealam, W.W. Kuo, M.A. Shibu, C.H. Day, ..., C.Y. Huang

Cardioprotective potential of amygdalin against angiotensin II induced cardiac hypertrophy, oxidative stress and inflammatory responses through modulation of Nrf2 and NF-κB activation

Environmental Toxicology, 36 (5) (2021), pp. 926-934

[Crossref ↗](#) [View in Scopus ↗](#) [Google Scholar ↗](#)

[Li, Chen, Li, Huang and Zhao, 2020](#) F. Li, Y. Chen, Y. Li, M. Huang, W. Zhao

Geniposide alleviates diabetic nephropathy of mice through AMPK/SIRT1/NF-κB pathway

European Journal of Pharmacology, 886 (2020), Article 173449

 [View PDF](#) [View article](#) [View in Scopus ↗](#) [Google Scholar ↗](#)

[Li et al., 2022](#) Y. Li, R. Wan, J. Liu, W. Liu, L. Ma, H. Zhang

In silico mechanisms of arsenic trioxide-induced cardiotoxicity

Frontiers in Physiology, 13 (2022), p. 1004605

[View in Scopus ↗](#) [Google Scholar ↗](#)

[Liang et al., 2020](#) Y. Liang, B. Zheng, J. Li, J. Shi, L. Chu, X. Han, ..., J. Zhang
Crocic ameliorates arsenic trioxide-induced cardiotoxicity via Keap1-Nrf2/HO-1 pathway: Reducing oxidative stress, inflammation, and apoptosis
Biomedicine & Pharmacotherapy, 131 (2020), Article 110713

 [View PDF](#) [View article](#) [View in Scopus ↗](#) [Google Scholar ↗](#)

[Liczbiński and Bukowska, 2018](#) P. Liczbiński, B. Bukowska
Molecular mechanism of amygdalin action in vitro: Review of the latest research

Immunopharmacology and Immunotoxicology, 40 (3) (2018), pp. 212-218

[View in Scopus ↗](#) [Google Scholar ↗](#)

[Liu et al., 2020](#) J. Liu, Y. Yuan, X. Gong, L. Zhang, Q. Zhou, S. Wu, ..., X. Yin, *et al.*
Baicalin and its nanoliposomes ameliorates nonalcoholic fatty liver disease via suppression of TLR4 signaling cascade in mice

International Immunopharmacology, 80 (2020), Article 106208

 [View PDF](#) [View article](#) [View in Scopus ↗](#) [Google Scholar ↗](#)

[Liu et al., 2021](#) P. Liu, J. Li, M. Liu, M. Zhang, Y. Xue, Y. Zhang, ..., L. Chu
Hesperetin modulates the Sirt1/Nrf2 signaling pathway in counteracting myocardial ischemia through suppression of oxidative stress, inflammation, and apoptosis

Biomedicine & Pharmacotherapy, 139 (2021), Article 111552

 [View PDF](#) [View article](#) [View in Scopus ↗](#) [Google Scholar ↗](#)

[Liu et al., 2021](#) S. Liu, A. Xu, Y. Gao, Y. Xie, Z. Liu, M. Sun, ..., X. Wang
Graphene oxide exacerbates dextran sodium sulfate-induced colitis via ROS/AMPK/p53 signaling to mediate apoptosis

Journal of Nanobiotechnology, 19 (1) (2021), p. 85

 [View PDF](#) [View article](#) [Crossref ↗](#) [Google Scholar ↗](#)

[Liu et al., 2022](#) X. Liu, M. Li, Z. Chen, Y. Yu, H. Shi, Y. Yu, ..., J. Ge
Mitochondrial calpain-1 activates NLRP3 inflammasome by cleaving ATP5A1 and inducing mitochondrial ROS in CVB3-induced myocarditis

Basic Research in Cardiology, 117 (1) (2022), p. 40

[Google Scholar ↗](#)

[Liu, Liu, Tang and Du, 2023](#) X. Liu, Y. Liu, L. Tang, C. Du

Inhibition of farnesyl pyrophosphate synthase alleviates cardiomyopathy in diabetic rat

Cell cycle (Georgetown, Tex), 22 (6) (2023), pp. 666-679

[Crossref ↗](#) [View in Scopus ↗](#) [Google Scholar ↗](#)

[Liu et al., 2022](#) Y. Liu, J. Shu, T. Liu, J. Xie, T. Li, H. Li, L. Li

Nicorandil protects against coronary microembolization-induced myocardial injury by suppressing cardiomyocyte pyroptosis via the AMPK/TXNIP/NLRP3 signaling pathway

European Journal of Pharmacology, 936 (2022), Article 175365

 [View PDF](#) [View article](#) [View in Scopus ↗](#) [Google Scholar ↗](#)

[Lu, Wang, Han and Li, 2023](#) J.S. Lu, J.H. Wang, K. Han, N. Li

Nicorandil regulates Ferroptosis and mitigates septic cardiomyopathy via TLR4/SLC7A11 signaling pathway

Inflammation, 47 (3) (2023), pp. 975-988

[View in Scopus ↗](#) [Google Scholar ↗](#)

[Mandlik, Mandlik and Patel, 2021](#) D.S. Mandlik, S.K. Mandlik, S. Patel

Protective effect of sarsasapogenin in TNBS induced ulcerative colitis in rats associated with downregulation of pro-inflammatory mediators and oxidative stress

Immunopharmacology and Immunotoxicology, 43 (5) (2021), pp. 571-583

[Crossref ↗](#) [View in Scopus ↗](#) [Google Scholar ↗](#)

[Park et al., 2023](#) J.H. Park, J. Lee, G.R. Lee, M. Kwon, H.I. Lee, N. Kim, ..., W. Jeong

Cholesterol sulfate inhibits osteoclast differentiation and survival by regulating the AMPK-Sirt1-NF- κ B pathway

Journal of Cellular Physiology, 238 (9) (2023), pp. 2063-2075

[Crossref ↗](#) [View in Scopus ↗](#) [Google Scholar ↗](#)

[Pei, Wen, Cui, Yang and Xie, 2021](#) X. Pei, Y. Wen, F. Cui, Z. Yang, Z. Xie

lncRNA CASC7 regulates pathological progression of ox-LDL-stimulated atherosclerotic cell models via sponging miR-21 and regulating PI3K/Akt and TLR4/NF- κ B signaling pathways

Aging, 13 (23) (2021), pp. 25408-25425

[Crossref ↗](#) [View in Scopus ↗](#) [Google Scholar ↗](#)

[Pohjoismäki and Goffart, 2017](#) J.L. Pohjoismäki, S. Goffart

The role of mitochondria in cardiac development and protection

Free Radical Biology and Medicine, 106 (2017), pp. 345-354



[View PDF](#) [View article](#) [View in Scopus ↗](#) [Google Scholar ↗](#)

[Qiao, Zhang, Liu, Xu and Li, 2022](#) P. Qiao, B. Zhang, X. Liu, J. Xu, X. Li

Effects of Escin on oxidative stress and apoptosis of H9c2 cells induced by H₂O₂

Disease Markers, 2022 (2022), p. 7765353

[View in Scopus ↗](#) [Google Scholar ↗](#)

[Rabinovich-Nikitin, Blant, Dhingra, Kirshenbaum and Czubryt, 2022](#) I. Rabinovich-Nikitin, A. Blant,

R. Dhingra, L.A. Kirshenbaum, M.P. Czubryt

NF- κ B p65 attenuates cardiomyocyte PGC-1 α expression in hypoxia

Cells, 11 (14) (2022)

[Google Scholar ↗](#)

[Saleem, Asif, Asif and Saleem, 2018](#) M. Saleem, J. Asif, M. Asif, U. Saleem

Amygdalin from apricot kernels induces apoptosis and causes cell cycle arrest in Cancer cells: An updated review

Anti-Cancer Agents in Medicinal Chemistry, 18 (12) (2018), pp. 1650-1655

[View in Scopus ↗](#) [Google Scholar ↗](#)

[Shan et al., 2019](#) S. Shan, R. Liu, H. Feng, Y. Zhang, F. Zhang, C. Lv, G. Yang

Identification and functional characterization of the transcription factor NF- κ B subunit p65 in common carp (*Cyprinus carpio* L.)

Fish & Shellfish Immunology, 95 (2019), pp. 25-34



[View PDF](#) [View article](#) [View in Scopus ↗](#) [Google Scholar ↗](#)

[Singh, Goel and Kaur, 2011](#) A.P. Singh, R.K. Goel, T. Kaur

Mechanisms pertaining to arsenic toxicity

Toxicology International, 18 (2) (2011), pp. 87-93

[View in Scopus ↗](#) [Google Scholar ↗](#)

[Song and Zhou, 2022](#) B. Song, W. Zhou

Amarogentin has protective effects against sepsis-induced brain injury via modulating the AMPK/SIRT1/NF- κ B pathway

Brain Research Bulletin, 189 (2022), pp. 44-56



[View PDF](#) [View article](#) [View in Scopus ↗](#) [Google Scholar ↗](#)

[Su et al., 2019](#) X. Su, Z. Shen, Q. Yang, F. Sui, J. Pu, J. Ma, ..., P. Hou

Vitamin C kills thyroid cancer cells through ROS-dependent inhibition of MAPK/ERK and PI3K/AKT pathways via distinct mechanisms

Theranostics, 9 (15) (2019), pp. 4461-4473

[Crossref ↗](#) [View in Scopus ↗](#) [Google Scholar ↗](#)

[Te Lintel et al., 2021](#) H.M. Te Lintel, G. Newton, K. Chapman, R. Aqil, R. Downham, R. Yan, ..., D. Cawkill, *et al.*

Preclinical trial of a MAP4K4 inhibitor to reduce infarct size in the pig: Does cardioprotection in human stem cell-derived myocytes predict success in large mammals?

Basic Research in Cardiology, 116 (1) (2021), p. 34

[Google Scholar ↗](#)

[Thompson, Davison, Crawford and Hughes, 2022](#) G. Thompson, G.W. Davison, J. Crawford, C.M. Hughes

Exercise and Cardioprotection in coronary artery disease: A pilot quasi-experimental study

Journal of Aging and Physical Activity, 30 (2) (2022), pp. 281-296

[Crossref ↗](#) [View in Scopus ↗](#) [Google Scholar ↗](#)

[Tian et al., 2019](#) L. Tian, W. Cao, R. Yue, Y. Yuan, X. Guo, D. Qin, ..., X. Wang

Pretreatment with Tiliarin improves mitochondrial energy metabolism and oxidative stress in rats with myocardial ischemia/reperfusion injury via AMPK/SIRT1/PGC-1 alpha signaling pathway

Journal of Pharmacological Sciences, 139 (4) (2019), pp. 352-360

 [View PDF](#) [View article](#) [View in Scopus ↗](#) [Google Scholar ↗](#)

[Vineetha and Raghu, 2019](#) V.P. Vineetha, K.G. Raghu

An overview on arsenic trioxide-induced cardiotoxicity

Cardiovascular Toxicology, 19 (2) (2019), pp. 105-119

[Crossref ↗](#) [View in Scopus ↗](#) [Google Scholar ↗](#)

[Wang et al., 2022](#) B. Wang, T. Sun, L. Sun, L. Li, H. Wan, Z. Ding, X. Ye

Amygdalin attenuates PM2.5-induced human umbilical vein endothelial cell injury via the TLR4/NF-κB and Bcl-2/Bax signaling pathways

Acta Biochimica et Biophysica Sinica, 54 (10) (2022), pp. 1476-1485

[Crossref ↗](#) [View in Scopus ↗](#) [Google Scholar ↗](#)

[Wang et al., 2020](#) C. Wang, Y. Gao, Z. Zhang, Q. Chi, Y. Liu, L. Yang, K. Xu

Safflower yellow alleviates osteoarthritis and prevents inflammation by inhibiting PGE2 release and regulating NF- κ B/SIRT1/AMPK signaling pathways

Phytomedicine: international journal of phytotherapy and phytopharmacology, 78 (2020), Article 153305



[View PDF](#) [View article](#) [View in Scopus](#) [Google Scholar](#)

[Wang et al., 2025](#) L. Wang, S. Liu, C. Gao, H. Chen, J. Li, J. Lu, ..., X. Zhang, *et al.*

Arsenic trioxide-induced cardiotoxicity triggers ferroptosis in cardiomyoblast cells. (1477–0903 (Electronic)) (2025)

[Google Scholar](#)

[Wu et al., 2022](#) Z. Wu, H. Chen, L. Lin, J. Lu, Q. Zhao, Z. Dong, X. Hai

Sacubitril/valsartan protects against arsenic trioxide induced cardiotoxicity in vivo and in vitro

Toxicology Research, 11 (3) (2022), pp. 451-459

[Crossref](#) [View in Scopus](#) [Google Scholar](#)

[Xue et al., 2020](#) Y. Xue, M. Li, Y. Xue, W. Jin, X. Han, J. Zhang, ..., L. Chu

Mechanisms underlying the protective effect of tannic acid against arsenic trioxide-induced cardiotoxicity in rats: Potential involvement of mitochondrial apoptosis

Molecular Medicine Reports, 22 (6) (2020), pp. 4663-4674

[Crossref](#) [View in Scopus](#) [Google Scholar](#)

[Yang et al., 2019](#) B. Yang, H. Li, Y. Qiao, Q. Zhou, S. Chen, D. Yin, ..., M. He

Tetramethylpyrazine attenuates the Endotheliotoxicity and the mitochondrial dysfunction by doxorubicin via 14-3-3 γ /Bcl-2

Oxidative Medicine and Cellular Longevity, 2019 (2019), p. 5820415

[View in Scopus](#) [Google Scholar](#)

[Yang, Wang, Shi, Zhao and Li, 2022](#) M.H. Yang, Y.S. Wang, X.Q. Shi, X.W. Zhao, B. Li

Arsenic trioxide restrains lung Cancer growth and metastasis by blocking the Calcineurin-NFAT pathway by upregulating DSCR1

Current Cancer Drug Targets, 22 (10) (2022), pp. 854-864

[Google Scholar](#)

[Yang, Kahn, Shi and Xue, 2010](#) Z. Yang, B.B. Kahn, H. Shi, B.Z. Xue

Macrophage alpha1 AMP-activated protein kinase (alpha1AMPK) antagonizes fatty acid-induced inflammation through SIRT1

The Journal of Biological Chemistry, 285 (25) (2010), pp. 19051-19059

 [View PDF](#) [View article](#) [Crossref ↗](#) [View in Scopus ↗](#) [Google Scholar ↗](#)

[Ye et al., 2020](#) J. Ye, M. Wang, R. Wang, H. Liu, Y. Qi, J. Fu, ..., X. Sun

Hydroxysafflor yellow a inhibits hypoxia/reoxygenation-induced cardiomyocyte injury via regulating the AMPK/NLRP3 inflammasome pathway

International Immunopharmacology, 82 (2020), Article 106316

(Advance online publication)

 [View PDF](#) [View article](#) [View in Scopus ↗](#) [Google Scholar ↗](#)

[Zhang et al., 2018a](#) J. Zhang, M. Wang, R. Wang, X. Sun, Y. Du, J. Ye, ..., X. Sun

Salvianolic acid a ameliorates arsenic trioxide-induced cardiotoxicity through decreasing cardiac mitochondrial injury and promotes its anticancer activity

Frontiers in Pharmacology, 9 (2018), p. 487

[View in Scopus ↗](#) [Google Scholar ↗](#)

[Zhang, Zhang, Wang, Li and Zhang, 2018b](#) J. Zhang, Y. Zhang, W. Wang, C. Li, Z. Zhang

Double-sided personality: Effects of arsenic trioxide on inflammation

Inflammation, 41 (4) (2018), pp. 1128-1134

[Crossref ↗](#) [View in Scopus ↗](#) [Google Scholar ↗](#)

[Zhang et al., 2018b](#) J.Y. Zhang, M. Wang, R.Y. Wang, X. Sun, Y.Y. Du, J.X. Ye, ..., X.B. Sun

Salvianolic acid a ameliorates arsenic trioxide-induced cardiotoxicity through decreasing cardiac mitochondrial injury and promotes its anticancer activity

Frontiers in Pharmacology, 9 (2018), p. 487

[View in Scopus ↗](#) [Google Scholar ↗](#)

[Zhang et al., 2021](#) M. Zhang, Y. Xue, B. Zheng, L. Li, X. Chu, Y. Zhao, ..., Z. Wu, *et al.*

Liquiritigenin protects against arsenic trioxide-induced liver injury by inhibiting oxidative stress and enhancing mTOR-mediated autophagy

Biomedicine & Pharmacotherapy, 143 (2021), Article 112167

 [View PDF](#) [View article](#) [View in Scopus ↗](#) [Google Scholar ↗](#)

[Zhang et al., 2021](#) X. Zhang, B. Hu, Y.F. Sun, X.W. Huang, J.W. Cheng, A. Huang, ..., J. Fan, *et al.*

Arsenic trioxide induces differentiation of cancer stem cells in hepatocellular carcinoma through inhibition of LIF/JAK1/STAT3 and NF- κ B signaling pathways synergistically

Clinical and Translational Medicine, 11 (2) (2021), Article e335

[Google Scholar ↗](#)

[Zhang et al., 2021](#) X. Zhang, S. Lv, W. Zhang, Q. Jia, L. Wang, Y. Ding, ..., Y. Li, *et al.*

Shenmai injection improves doxorubicin cardiotoxicity via miR-30a/Beclin 1

Biomedicine & Pharmacotherapy, 139 (2021), Article 111582

 [View PDF](#) [View article](#) [View in Scopus ↗](#) [Google Scholar ↗](#)

[Zheng et al., 2013](#) C.Y. Zheng, S.K. Lam, Y.Y. Li, B.M. Fong, J.C. Mak, J.C. Ho

Combination of arsenic trioxide and chemotherapy in small cell lung cancer

Lung cancer (Amsterdam, Netherlands), 82 (2) (2013), pp. 222-230

 [View PDF](#) [View article](#) [View in Scopus ↗](#) [Google Scholar ↗](#)

[Zheng, Bian, Zhang, Ren and Li, 2020](#) Z. Zheng, Y. Bian, Y. Zhang, G. Ren, G. Li

Metformin activates AMPK/SIRT1/NF- κ B pathway and induces mitochondrial dysfunction to drive caspase3/GSDME-mediated cancer cell pyroptosis

Cell cycle (Georgetown, Tex), 19 (10) (2020), pp. 1089-1104

[Crossref ↗](#) [View in Scopus ↗](#) [Google Scholar ↗](#)

Cited by (0)

- 1 These authors contributed equally to this work.

© 2025 The Authors. Published by Elsevier Ltd.



